Journal of Biochemical and Molecular Toxicology

WILEY

RESEARCH ARTICLE OPEN ACCESS

Synthesis and Characterization of Schiff Bases and Their Ag(I) Complexes Containing 2,5,6-Trisubstituted Imidazothiadiazole Derivatives: Molecular Docking and In Vitro Cytotoxic Effects Against Nonsmall Lung Cancer Cell Line

Ahmed Hamdi Mirghani[1] | Suray Pehlivanoglu[2] | Hakan Alici[3] | Hakan Tahtaci[1] | Saban Uysal[1]

[1]Department of Chemistry, Science Faculty, Karabuk University, Karabuk, Turkey | [2]Department of Molecular Biology and Genetic, Science Faculty, Necmettin Erbakan University, Konya, Turkey | [3]Department of Physics, Faculty of Science, Zonguldak Bulent Ecevit University, Zonguldak, Turkey

Correspondence: Saban Uysal (sabanuysal@karabuk.edu.tr) | Ahmed Hamdi Mirghani (dr.ahmedabuharaz@gmail.com)

Received: 9 November 2024 | **Revised:** 26 December 2024 | **Accepted:** 4 January 2025

Funding: This study is funded by Karabük Üniversitesi.

Keywords: cytotoxic activity | imidazo[2,1-*b*][1,3,4]thiadiazole | molecular docking | silver complex | Vilsmeier–Haack reagent

ABSTRACT

In this study, four novels 2,5,6-trisubstituted imidazothiadiazole derivative ligands and their Ag(I) complexes were synthesized and characterized using various spectroscopic analysis techniques. First, imidazo[2,1-*b*][1,3,4]thiadiazole derivative **(3)** was obtained from the reaction of 5-amino-1,3,4-thiadiazole-2-thiol with benzyl bromide in the presence of KOH in an ethanolic medium. In the next step, the resultant compound reacted sequentially with four substituted phenacyl bromide derivatives **(4a–4d)** under refluxed ethanol for 24 h to obtain substituted 2-(benzylthio)-6-phenylimidazo[2,1-*b*][1,3,4]thiadiazole derivatives **(5–8)**. Compounds **(9–12)** were obtained by attaching a carbonyl group to carbon number 5 of the imidazothiadiazole group in these compounds with the help of Vilsmeier–Haack reagent. The resultant compounds were reacted in an ethanolic medium to synthesize the novel **(13–16)** ligands by adding ethylenediamine in a 1:2 molar ratio. The Ag(I) complexes of the resultant ligands were synthesized by mixing silver acetate with the ligands in a dimethyl sulfoxide medium to obtain **(17–20)** complexes. All the synthesized compounds were analyzed using FTIR, ^{1}H NMR, ^{13}C NMR, mass spectroscopy, magnetic susceptibility, ICP-OES, and thermogravimetric analysis techniques. The study also investigates the in vitro cytotoxic effect of the ligands and complexes on A549 (nonsmall cell lung cancer) cells using the MTT assay and shows that the **13**, **15**, and **16** ligands, together with their complexes, exhibit potent cytotoxicity. In addition, in silico molecular docking simulations were conducted both to support the in vitro cytotoxicity experiments and to ascertain the active binding sites and interactions of the ligands and complexes on the EGFR receptor. The result indicates that ligands and complexes may serve as promising candidates for further investigation as anticancer agents.

1 | Introduction

Today, drug resistance has become a global problem, prompting researchers to synthesize a new drug molecule and thiadiazole derivatives are one of them [1]. Thiadiazole pentacyclic compounds comprise two nitrogen atoms (containing a double electron), a sulfur atom, and two carbon atoms. Thiadiazoles are one of the most important heterocyclic compounds in recent

decades, and they have been of great interest in research due to their extensive biological activities [2–5]. Therefore, due to their high biological activity, these compounds and their derivatives are considered among the basic compounds used in the manufacture of commercial medicines, chemistry, and agriculture. They are found in nature with four isomers: 1,2,4-thiadazole, 1,2,3-thiadazole, 1,2,5-thiadazole, and 1,3,4-thiadazole [1, 6].

Numerous studies have shown the importance of thiadiazole derivatives as antibacterial, antifungal, anticancer, and anti-inflammatory, and because of the emerging of multidrug-resistance problems against mycobacterial infections. Thiadiazoles are important in the preparation of specific antibiotics like 2-(4-chlorophenylamino)-5-(4-aminophenyl)-1,3,4-thiadiazole which showed high anti-mycobacterial activity against *Mycobacterium tuberculosis* [7]. In 2019 Hakan Tahtaci and colleagues, successfully synthesized, characterized, and biological activity tested a novel derivative of the thidiazole compound. From their point of view 2-(4-fluorobenzylthio)-6-(4-fluorophenyl)imidazo[2,1-*b*][1,3,4]thiadiazole showed high antileishmanial activity, while 4-(2-(4-fluorobenzylthio)imidazo [2,1-*b*][1,3,4]thiadiazol-6-yl)benzonitrile, 2-(4-fluorobenzylthio)-6-(4-phenylphenyl)imidazo[2,1-*b*][1,3,4]thiadiazole, and 4-(2-(4-methoxybenzyl)imidazo[2,1-*b*][1,3,4]thiadiazol-6-yl)benzonitrile were effective at different concentrations [3, 8]. The biological activity of these compounds comes from the sulfur atom, hydrogen binding domain, and the two-electron donor nitrogen system, while conductivity and thermal properties come from sulfur and nitrogen atoms [9].

Among four isomers of thiadiazole, 1,3,4-thiadiazole is the highly reactive one while amino-1,3,4-thiadiazole derivatives have been used as starting material for the synthesis of anticancer agents [2, 10–13]. Some thiadiazole derivatives like Levamisole and Dexamisole enantiomers of Levamisole are used to enhance and improve the immune system's role [14–16]. Also one of the most important derivatives of these compounds is imidazo[2,1-*b*][1,3,4]thiadiazole because it has been considered a nonsteroidal cytotoxic agent and that's why used in the synthesis of many anticancer compounds [17–22].

Cancer is a multiple disease caused by limitless uncontrollable division of the cells and the affected cells can invade healthy ones in a process called metastasis. A couple of proteins are responsible for metastasis, one of these proteins is TGFβ receptors which triggers this process by receiving the phosphate group from adenosine triphosphate (ATP) and initiating the metastasis signaling [19, 23]. By binding imidazo[2,1-*b*][1,3,4] thiadiazole derivatives to TGFβ receptors they cancel the phosphorylation reaction and signals that trigger the metastasis, and all of this because of the similarity of these derivatives to ATP which will lead to binding of thiadiazoles to TGFβ receptors instead of ATP and making it anticancer agent [24–28].

Lung cancer remains a significant global health concern, responsible for a substantial number of deaths each year. As noted previously, it primarily divides into two categories: small cell lung cancer (SCLC) and nonsmall cell lung cancer (NSCLC). NSCLC accounts for about 85%–90% of lung cancer cases and is typically classified into subtypes, including adenocarcinoma, squamous cell carcinoma, and large cell carcinoma. These types originate from the epithelial cells lining the lungs [29]. Currently, lung cancer treatments include surgical resection, radiotherapy, and chemotherapy. However, molecular-targeted therapies offer promising alternatives that may enhance survival and quality of life for patients. Gefitinib is a selective inhibitor of the epidermal growth factor receptor (EGFR) tyrosine kinase which is one such targeted therapy. It has been shown to suppress tumor growth, metastasis, and angiogenesis in EGFR-positive cells. Also, its triggering apoptosis and increasing sensitivity to chemotherapy in the targeted treatment of lung cancer [30]. Although standard chemotherapy is effective for about 30% of lung cancer patients, resistance to chemotherapy is a common occurrence. The low response rate to chemotherapy has prompted scientists to develop new treatment regimens [29].

This study aims to synthesize four novel derivatives **(13–16)** of imidazo[2,1-*b*][1,3,4]thiadiazole, characterize their structures using various spectroscopic techniques, and evaluate their anticancer activity against NSCLC cells.

2 | Experimental

2.1 | Materials and Methods

All the chemicals and reagents (ethanol, 5-amino-1,3,4-thiadiazol-2-thiol, potassium hydroxide, benzyl bromide, potassium carbonate, *N*,*N*-dimethylformamide, 2-bromoacetophenone, 2-bromo-4-chloroacetophenone, 2-bromo-4-methylacetophenone, 2-bromo-4-methoxyacetophe- none, phosphoryl chloride, dichloromethane, sodium carbonate, sodium sulfate, ethylenediamine, dimethylsulfoxide, and silver acetate) used were brought from commercial suppliers (Merck and Sigma-Aldrich) which were used without any further purification. The reactions are monitored by thin-layer chromatography using silica gel plates (Merck). Melting points were determined by (Electrothermal M659160) using capillary tubes. UV light is used as a visualization agent. The FTIR spectra of each compound were detected on Thermo Scientific Nicolet IS5 with IS7 ATR apparatus. ^{1}H and ^{13}C NMR spectra were recorded on a BURKER 400 MHz spectrometer using $CDCl_3$ as a solvent. Elemental analysis of the ligands was performed using a LECO 932 CHNS analyzer from St. Joseph, MI, USA. The metal contents of each complex were determined on a Perkin Elmer Optima 7000DV Model inductively coupled plasma optical emission spectrophotometer (ICP-OES). Magnetic susceptibility measurements were carried out using the Gouy method with $Hg[Co(SCN)_4]$ as the calibrant on a Sherwood Scientific MX Gouy apparatus. Thermal analysis, including thermogravimetric analysis (TGA), was conducted using a HITACHI STA7300 thermal analysis system. The mass spectra of the ligands and complexes were determined by the ESI (+) method and a Thermo TSQ Quantum Access device was used.

2.2 | Synthesis of imidazo[2,1-*b*][1,3,4]thiadiazole Derivatives (2–5)

In a two-necked round-bottom flask, KOH (2.81 g, 50.00 mmol) was added to a solution of 5-amino-1,3,4-thiadiazole-2-thiol

(6.66 g, 50.00 mmol) **(1)** in ethyl alcohol. Benzyl bromide (5.96 mL, 50.00 mmol) **(2)** dissolved in 100 mL ethyl alcohol, was then added dropwise to the mixture using a dropping funnel. The reaction mixture was refluxed for 6 h. The product was then filtered through a sintered funnel and left to recrystallize from ethanol. The pure product **(3)** was then filtered and dried in a vacuum desiccator with silica gel [18].

The product was subsequently reacted with various phenacyl bromide substituents **(4a–4d)** (13.40 mmol) in an ethanolic medium and refluxed for 24 h; at the end of the reaction solvent evaporated and the yielded compounds were washed with 5% potassium carbonate solution, then filtered and recrystallized from ethanol (Scheme 1). The resulting compounds **(5–8)** were characterized using elemental analysis, FTIR, ^{1}H NMR, and ^{13}C NMR spectroscopy.

Compound 3: $C_9H_9N_3S_2$; M.W. = 223.31; Color: Yellow; Yield: 10.7836 g (96.6%); M.P.: 152°C–154°C; m/z = 223.02. FTIR (ATR, cm^{-1}): 3278 (NH_2), 3098 (C–$H_{ar.}$), 1641 (C=N_{thia}), and 694 (C–S). ^{1}H NMR (400 MHz, DMSO) δ 7.37–7.36 (d, 2H) $CH_{ar.}$, 7.35–7.34 (d, 2H) $CH_{ar.}$, 7.32 (s, 2H) NH_2, 7.28–7.26 (d, 2H) $CH_{ar.}$, 4.30 (s, 2H) SCH_2. ^{13}C NMR (100 MHz, DMSO) δ 170.34 (C–NH_2), 149.97 (C=N), (137.57, 129.45, 128.95, 127.91) C–C $_{ar.}$, 38.94 (C–S).

Compound 5: $C_{17}H_{13}N_3S_2$; M.W. = 323.43; Color: White; Yield: 3.9671 g (91.4%); M.P.: 144°C–147°C; m/z = 323.06. FTIR (ATR, cm^{-1}): 3048 (C–$H_{ar.}$), 1601 (C=$N_{imthd.}$), 1022 ($^{}$N–N), 691 (C–S). ^{1}H NMR (400 MHz, $CDCl_3$) δ 7.95 (s, 1H)$_{imthd.}$, 7.80–7.79 (d, 2H) $CH_{ar.}$, 7.42–7.25 (m, 8H) $CH_{ar.}$, 4.44 (s, 2H) SCH_2. ^{13}C NMR (100 MHz, $CDCl_3$) δ 159.17, 135.09, 133.78, 129.16, 129.02, 128.93, 128.77, 128.26, 127.60, 125.04, 38.78. Elem. Anal. Calculated/Found: C: 63.13/63.08, H: 4.05/3.99, N: 12.99/12.93, S: 19.82/19.77.

Compound 6: $C_{17}H_{12}ClN_3S_2$; M.W. = 357.87; Color: White; Yield: 4.2356 g (88.2%); M.P.: 168°C–170°C; m/z = 357.02. FTIR (ATR, cm^{-1}): 3034 cm^{-1} (C–$H_{ar.}$), 1598 cm^{-1} (C=$N_{imthd.}$), 1087 cm^{-1} ($^{}$N–N), 694 cm^{-1} (C–S). ^{1}H NMR (400 MHz, $CDCl_3$) δ 7.92 (s, 1H)$_{imthd.}$, 7.72–7.70 (d, 2H) $CH_{ar.}$, 7.40–7.25 (m, 7H) $CH_{ar.}$, 4.44 (d, 2H) SCH_2. ^{13}C NMR (100 MHz, $CDCl_3$) δ 159.53, 145.46, 144.88, 135.02, 133.20, 132.33, 129.15, 128.93, 128.28, 126.25, 38.73. Elem. Anal. Calculated/Found: C: 57.06/57.01, H: 3.83/3.78, N: 11.74/11.69, S: 17.92/17.87.

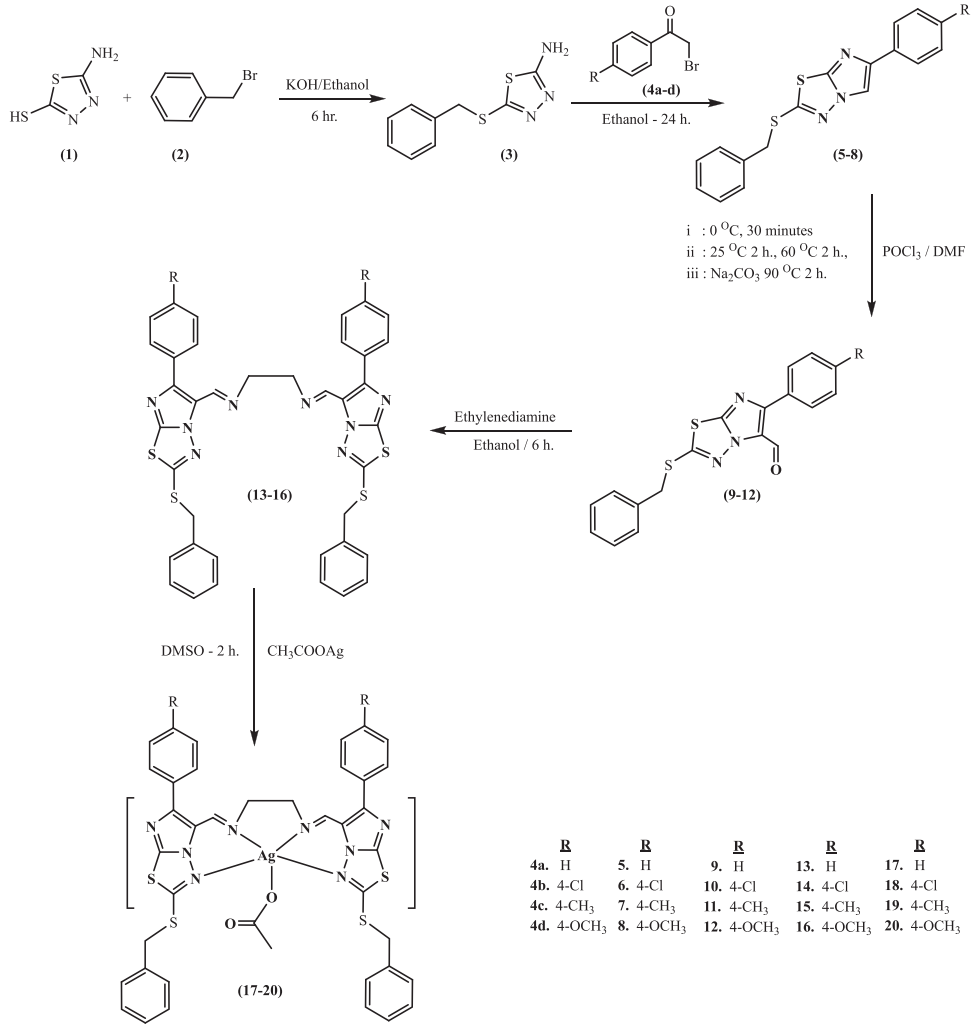

SCHEME 1 | Synthesis of all ligands and complexes.

Compound 7: $C_{17}H_{12}ClN_3S_2$ M.W. = 337.46; Color: White; Yield: 4.0134 g (88.75%); M.P.: 163°C–166°C; m/z = 337.07. FTIR (ATR, cm^{-1}): 3028 cm^{-1} (C-$H_{ar.}$), 1601 cm^{-1} (C=$N_{imthd.}$), 1069 cm^{-1} (N–N), 695 cm^{-1} (C–S). ^1H NMR (400 MHz, $CDCl_3$) δ 7.93 (s, 1H)$_{imthd.}$, 7.69 (dd, J = 8.2, 1.9 Hz, 2H) ar.CH, 7.39 (d, J = 7.8 Hz, 2H) $CH_{ar.}$, 7.34 (d, J = 7.8 Hz, 3H) $CH_{ar.}$, 7.22 (d, J = 8.2 Hz, 2H) $CH_{ar.}$, 4.45 (s, J = 2.0 Hz, 2H) SCH_2, 2.38 (s, 3H) CH_3. ^{13}C NMR (100 MHz, $CDCl_3$) δ 158.88, 146.09, 145.15, 137.40, 135.10, 130.92, 129.44, 129.13, 128.89, 128.22, 124.93, 108.95, 38.81, 21.26. Elem. Anal. Calculated/Found: C: 64.07/64.01, H: 4.84/4.79, N: 12.45/12.40, S: 19./18.95.

Compound 8: $C_{18}H_{15}N_3OS_2$; M.W. = 353.46; Color: White; Yield: 4.2569 g (89.9%); M.P.: 146°C–149°C; m/z = 353.07. FTIR (ATR, cm^{-1}): 3038 cm^{-1} (C–$H_{ar.}$), 1612 cm^{-1} (C=$N_{imthd.}$), 1073 cm^{-1} (N–N), 693 cm^{-1} (C–S). ^1H NMR (400 MHz, $CDCl_3$) δ 7.87 (s, 1H)$_{imthd.}$. CH, 7.70–7.72 (t, 2H) $CH_{ar.}$, 7.40–7.23 (m, 5H) $CH_{ar.}$, 6.93–6.95 (d, J = 6.6 Hz, 2H) $CH_{ar.}$, 4.44 (d, J = 2.1 Hz, 2H) SCH_2, 3.84 (s, 3H) OCH_3. ^{13}C NMR (100 MHz, $CDCl_3$) δ 159.37, 145.51, 145.02, 135.03, 129.12, 128.90, 128.24, 126.35, 126.08, 114.21, 108.43, 55.33, 38.86. Elem. Anal. Calculated/Found: C: 61.17/61.11, H: 4.28/4.22, N: 11.89/11.83, S: 18.14/18.09.

2.3 | Synthesis of 2-(Benzylthio)-6-phenylimidazo [2,1-*b*][1,3,4]thiadiazol-5-carbaldehyde Derivatives (6–9)

The Vilsmeier–Haack reagent is prepared by carefully adding phosphoryl chloride (2.00 mL, 21.00 mmol) to DMF (8.00 mL, 103.00 mmol) at 0°C with continuous stirring. Compounds **(5–8)** (4.50 mmol) were added separately to this reagent while maintaining the temperature at 0°C for the first 30 min. The temperature was then increased to room temperature for 2 h, and finally to 60°C for another 2 h. The reaction mixture was then poured into a sodium carbonate solution and stirred at 90°C for 2 h. After cooling to room temperature, the mixture was suspended with water and extracted three times with dichloromethane. The collected extracts were washed with water and dried with sodium sulfate. After filtration, the solvent was evaporated using a rotary evaporator, and the resulting solids **(9–12)** were recrystallized from dichloromethane (Scheme 1) [31]. The resulting compounds were characterized using elemental analysis, FTIR, ^1H NMR, and ^{13}C NMR spectroscopy.

Compound 9: $C_{18}H_{13}N_3S_2O$; M.W. = 351.44; Color: White; Yield: 1.3159 g (83.3%); M.P.: 138°C–140°C; m/z = 351.05. FTIR (ATR, cm^{-1}): 3056 cm^{-1} (C–$H_{ar.}$), 1669 cm^{-1} (C=O), 1092 cm^{-1} (N–N), 694 cm^{-1} (C–S). ^1H NMR (400 MHz, $CDCl_3$) δ 10.05 (s, 1H) O=CH, 7.86–7.84 (d, 2H) $CH_{ar.}$, 7.52–7.46 (m, 5H) $CH_{ar.}$, 7.37–7.29 (m, 3H) $CH_{ar.}$, 4.55 (s, 2H) SCH_2. ^{13}C NMR (100 MHz, $CDCl_3$) δ 177.37, 162.42, 155.58, 150.65, 134.75, 132.22, 129.83, 129.48, 129.10, 128.91, 128.86, 128.35, 124.16, 38.67. Elem. Anal. Calculated/Found: C: 61.52/61.48, H: 3.73/3.69, N: 11.96/11.91, S: 18.24/18.19.

Compound 10: $C_{18}H_{12}ClN_3S_2O$; M.W. = 385.88; Color: Yellow; Yield: 1.4329 g (82.4%); M.P.: 117°C–121°C; m/z = 385.01. FTIR (ATR, cm^{-1}): 3058 cm^{-1} (C–$H_{ar.}$), 1674 cm^{-1} (C=O), 1089 cm^{-1} (N–N), 691 cm^{-1} (C–S). ^1H NMR (400 MHz, $CDCl_3$) δ 10.07 (s, 1H) O=CH, 7.88–7.86 (d, 2H) $CH_{ar.}$, 7.46–7.44 (d, 4H) $CH_{ar.}$, 7.37–7.29 (m, 3H) $CH_{ar.}$, 4.54 (s, 2H) SCH_2. ^{13}C NMR (100 MHz, $CDCl_3$) δ 177.01, 162.75, 153.42, 150.25, 136.00, 134.67, 130.73, 130.19, 129.44, 129.02, 128.93, 128.40, 124.03, 38.63. Elem. Anal. Calculated/Found: C: 56.03/55.98, H: 3.13/3.08, N: 10.89/10.85, S: 16.62/16.57.

Compound 11: $C_{19}H_{15}N_3S_2O$; M.W. = 365.47; Color: Yellow; Yield: 1.5435 g (94%); M.P.: 128°C–130°C; m/z = 365.07. FTIR (ATR, cm^{-1}): 3031 cm^{-1} (C–$H_{ar.}$), 1654 cm^{-1} (C=O), 1069 cm^{-1} (N–N), 694 cm^{-1} (C–S). ^1H NMR (400 MHz, $CDCl_3$) δ 10.03 (s, 1H) O=CH, 7.73–7.75 (d, 2H) $CH_{ar.}$, 7.45–7.47 (d, 2H) $CH_{ar.}$, 7.36–7.29 (m, 5H) $CH_{ar.}$, 4.54 (s, 2H) SCH_2, 2.42 (s, 3H) CH_3. ^{13}C NMR (100 MHz, $CDCl_3$) δ 177.35, 162.12, 155.81, 150.63, 140.07, 134.76, 129.57, 129.46, 129.38, 128.97, 128.88, 128.31, 123.99, 38.66, 21.42. Elem. Anal. Calculated/Found: C: 62.44/62.39, H: 4.14/4.10, N: 11.50/11.44, S: 17.54/17.49.

Compound 12: $C_{19}H_{15}N_3S_2O_2$; M.W. = 381.47; Color: Yellow; Yield: 1.5628 g (91%); M.P.: 142°C–144°C; m/z = 381.06. FTIR (ATR, cm^{-1}): 3006 cm^{-1} (C–$H_{ar.}$), 1667 cm^{-1} (C=O), 1054 cm^{-1} (N–N), 695 cm^{-1} (C–S). ^1H NMR (400 MHz, $CDCl_3$) δ 10.03 (s, 1H) O=CH, 7.85–7.82 (d, J = 8.8 Hz, 2H) $CH_{ar.}$, 7.45–7.46 (d, J = 6.9 Hz, 2H) $CH_{ar.}$, 7.33–7.30 (m, 3H) $CH_{ar.}$, 7.00–7.02 (d, J = 8.8 Hz, 2H) $CH_{ar.}$, 4.54 (s, 2H) SCH_2, 3.86 (d, J = 2.0 Hz, 3H) OCH_3. ^{13}C NMR (100 MHz, $CDCl_3$) δ 177.25, 161.88, 161.04, 155.42, 150.52, 134.76, 130.45, 129.43, 128.89, 128.32, 124.75, 123.71, 114.27, 55.41, 38.69. Elem. Anal. Calculated/Found: C: 59.82/59.77, H: 3.96/3.93, N: 11.02/10.97, S: 16.81/16.75.

2.4 | Synthesis of Ligands (13–16)

In a round-bottom flask, ethylene diamine (0.5 mmol) was added under reflux to 5-formyl imidazo[2,1-*b*][1,3,4] thiadiazole derivatives (1 mmol) in an ethanolic medium (50 mL) for 6 h. At the end of the reaction, the solid yield **(13–16)** ligands were filtered out, washed with cold ethanol, and left to dry (Scheme 1). Elemental analysis, FTIR, ^1H NMR, ^{13}C NMR, and mass spectroscopy characterized the resulting compounds.

Ligand 13: $C_{38}H_{30}N_8S_4$; M.W. = 726.95 g/mol; Color: Yellow; Yield: 0.3436 g (94.5%); M.P.: 126°C–129°C; ESI m/z = 726.15. FTIR (ATR, cm^{-1}): 2831, 2880, 2906 (C–$H_{al.}$), 3029, 3055 (C–$H_{ar.}$), 1626 (C=$N_{im.}$), 1400, 1437, 1450 (C=C_{ar}), 1526, 1576, 1600 (C=$N_{imthd.}$, and C=$C_{imthd.}$) 659, 692 (C–S); ^1H NMR (400 MHz, $CDCl_3$) δ 8.45 (s, 2H) N=CH, 7.60–7.58 (dd, 4H) $CH_{ar.}$, 7.35–7.33 (d, J = 6.4 Hz, 4H), 7.26–7.19 (m, 12H) $CH_{ar.}$, 4.30 (s, 4H) SCH_2, 4.05 (s, 4H) NCH_2; ^{13}C NMR (100 MHz, $CDCl_3$) δ 160.29 (C=$N_{imthd.}$), 150.56 (C=$N_{im.}$), 149.12, and 147.90 (C=$C_{imthd.}$), 135.13, and 133.35 (C=$N_{imthd.}$), 129.48, 128.80, 128.63, 128.51, 128.44, and 128.19 (C–$C_{ar.}$), 121.69 (C–$N_{imthd.}$), 62.73 (C–N), 38.53 (C–S). Elem. Anal. Calculated/Found: C: 62.78/62.73, H: 4.16/4.11, N: 15.41/15.37, S: 17.64/17.60.

Ligand 14: $C_{38}H_{28}Cl_2N_8S_4$; M.W. = 795.84 g/mol; Color: Yellow; Yield: 0.3775 g (94.87%); M.P.: 159°C–162°C; ESI m/z = 794.07. FTIR (ATR, cm^{-1}): 2849, 2876, 2912 (C–$H_{al.}$), 3028 (C–$H_{ar.}$), 1625 (C=$N_{im.}$), 1446,1460,1495 (C=$C_{ar.}$), 1518, 1568 (C=$N_{imthd.}$, and C=$C_{imthd.}$) 635, 675, 696 (C–S); ^1H NMR

(400 MHz, DMSO-d_6) δ 8.47 (s, 2H) N=CH, 7.87–7.85 (d, 4H) $CH_{ar.}$, 7.50–7.49 (d, 4H) $CH_{ar.}$, 7.31–7.24 (m, $J = 7.3$ Hz, 10H) $CH_{ar.}$.CH, 4.49 (s, 4H) SCH_2, 4.06 (s, 4H) NCH_2.; ^{13}C NMR (100 MHz, $CDCl_3$) δ 159.69 (C=N $_{imthd.}$), 149.29 (C=N $_{im.}$), 146.34 (C=$C_{imthd.}$), 133.95, 133.40 (C=$N_{imthd.}$), 130.78, 129.18, 128.74, 128.39, 127.81, 127.55, and 127.23 (C–$C_{ar.}$), 120.60 (C–$N_{imthd.}$), 61.56 (C–N), 37.63 (C–S). Elem. Anal. Calculated/Found: C: 57.35/57.31, H: 3.55/3.51, N: 14.08/14.01, S: 16.11/16.06.

Ligand 15: $C_{40}H_{34}N_8S_4$; M.W. = 755.01 g/mol; Color: Yellow; Yield: 0.3499 g (92.69%); M.P.:82°C–85°C; ESI m/z = 754.18. FTIR (ATR, cm^{-1}): 2866, 2916, 2972 (C–$H_{al.}$), 3026 (C–$H_{ar.}$), 1622 (C=$N_{im.}$), 1400, 1439, 1474 (C=$C_{ar.}$), 1536, 1574 (C=$N_{imthd.}$, and C=$C_{imthd.}$) 614, 667, 695 (C–S); ^{1}H NMR (400 MHz, $CDCl_3$) δ 8.43 (s, 2H) N=CH, 7.49–7.47 (d, $J = 8.1$ Hz, 4H) $CH_{ar.}$, 7.33–7.34 (d, $J = 6.3$ Hz, 4H) $CH_{ar.}$, 7.22–7.18 (t, 6H) $CH_{ar.}$, 7.06–7.04 (d, $J = 7.8$ Hz, 4H) $CH_{ar.}$, 4.29 (s, 4H) SCH_2, 4.04 (s, 4H) NCH_2, 2.27 (s, 6H) CH_3.; ^{13}C NMR (100 MHz, $CDCl_3$) δ 158.98 (C=N $_{imthd.}$), 149.61, and 148.28 (C=N $_{im.}$), 146.81 (C=C $_{imthd.}$), 137.36, and 134.12 (C=N $_{imthd.}$), 129.46, 128.45, 128.21, 127.75, 127.48, and 127.12 (C–$C_{ar.}$), 120.45 (C–$N_{imthd.}$), 61.46 (C–N), 37.68 (C–S), 20.40 (CH_3). Elem. Anal. Calculated/Found: C: 63.63/63.59, H: 4.54/4.50, N: 14.84/14.80, S: 16.99/16.94.

Ligand 16: $C_{40}H_{34}N_8S_4O_2$; M.W. = 787.01 g/mol; Color: Yellow; Yield: 0.3728 g (94.74%); M.P.: 176°C–178°C; ESI m/z = 786.17. FTIR (ATR, cm^{-1}): 2832, 2927, 2960 (C–$H_{al.}$), 3043 (C–$H_{ar.}$), 1644 (C=$N_{im.}$), 1436, 1495 (C=$C_{ar.}$), 1527, 1574 (C=$N_{imthd.}$, and C=$C_{imthd.}$) 640, 664 (C–S); ^{1}H NMR (400 MHz, $CDCl_3$) δ 8.41 (s, 2H) N=CH, 7.56–7.54 (d, $J = 8.8$ Hz, 4H) $CH_{ar.}$, 7.35–7.33 (d, 4H) $Ch_{ar.}$, 7.24–7.18 (m, 6H) $CH_{ar.}$, 6.76–6.75 (d, $J = 8.8$ Hz, 4H) $CH_{ar.}$, 4.30 (s, 4H) SCH_2, 4.05 (s, 4H) NCH_2, 3.71 (s, 6H) OCH_3; ^{13}C NMR (100 MHz, $CDCl_3$) δ 158.84 (C=$N_{imthd.}$), 149.71, 148.00 (C=$N_{im.}$), 146.64 (C=$C_{imthd.}$), 134.12 (C=$N_{imthd.}$), 128.85, 128.44, 127.76, 127.14, 124.88, 120.10, 113.26, and 112.90 (C–$C_{ar.}$), 61.65 (C–N), 54.39 (O–CH_3), 37.70 (C–S). Elem. Anal. Calculated/Found: C: 61.05/61.00, H: 4.35/4.29, N: 14.24/14.20, S: 16.29/16.24.

2.5 | Synthesis of Ag(I) Complexes (17–20)

Ligands containing heterocyclic compounds (0.50 mmol) were mixed with (0.0835 g, 0.50 mmol) $Ag(CH_3COO)$ in a 1:1 equivalent ratio in dimethyl sulfoxide medium at 65°C for 2 h. to obtain complex structures. The resulting complexes were crystallized and purified in the same medium. Subsequently, the structures of all these coordination compounds were characterized using elemental analysis, ICP-OES, FTIR, mass spectroscopy, and TGA methods. Due to the d^{10} electronic configuration of Ag(I) complexes, they generally preferred tetrahedral geometry. Ag(I) complexes also formed diamagnetic complexes due to their electronic structure.

Complex 17: $C_{40}H_{33}N_8O_2S_4Ag$; M.W. = 834.82, μ_{eff}: Dia.; Color: Orange; D.P.: 97°C–100°C; m/z = 892.07; FTIR (ATR, cm^{-1}): 2939, 2884, 2819 (C–$H_{al.}$), 3026, 3052 (C–$H_{ar.}$), 1671 $(C{=}O)_{acetate}$, 1642 (C=$N_{im.}$), 1419, 1434, 1481 (C–$C_{ar.}$), 1507, 1597 (C=$N_{imthd.}$, and C=$C_{imthd.}$) 617, 651 (C–S). Elem. Anal. Calculated/Found: C: 54.67/54.63, H: 3.62/3.57, N: 13.42/13.37, S: 15.36/15.32, Ag: 12.92/12.88.

Complex 18: $C_{40}H_{31}Cl_2N_8O_2S_4Ag$; M.W. = 903.71; μ_{eff}: Dia.; Color: Brown; D.P.: 162°C–164°C; m/z = 859.09; FTIR (ATR, cm^{-1}): 2834, 2872, 2900 (C–$H_{al.}$), 3026, 3060 (C–$H_{ar.}$), 1681 $(C{=}O)_{acetate}$, 1640 (C=$N_{im.}$), 1406, 1434, 1452 (C–$C_{ar.}$), 1510, 1564, 1599 (C=$N_{imthd.}$, and C=$C_{imthd.}$) 632, 666 (C–S). Elem. Anal. Calculated/Found: C: 50.51/50.47, H: 3.12/3.07, N: 12.40/12.37, S: 14.19/14.15, Ag: 11.94/11.90.

Complex 19: $C_{42}H_{37}N_8O_2S_4Ag$; M.W. = 862.88; μ_{eff}: Dia.; Color: Brown; D.P.: 116°C–118°C; m/z = 920.10; FTIR (ATR, cm^{-1}): 2830, 2867, 2898 (C–$H_{al.}$), 3032 (C–$H_{ar.}$), 1668 $(C{=}O)_{acetate}$, 1642 (C=$N_{im.}$), 1440, 1442, 1497 (C–$C_{ar.}$), 1532 (C=$N_{imthd.}$, and C=$C_{imthd.}$), 664, 698 (C–S). Elem. Anal. Calculated/Found: C: 55.68/55.63, H: 3.97/3.94, N: 12.99/12.95, S: 14.86/14.81, Ag: 12.50/12.46.

Complex 20: $C_{42}H_{37}N_8O_4S_4Ag$; M.W. = 894.87; μ_{eff}: Dia.; Color: Orange; D.P.: 104°C–106°C; m/z = 952.09; FTIR (ATR, cm^{-1}): 2832, 2931, 2958 (C–$H_{al.}$), 3005, 3085 (C–$H_{ar.}$), 1668 $(C{=}O)_{acetate}$, 1644 (C=$N_{im.}$), 1434, 1451, 1480 (C–$C_{ar.}$), 1522, 1576 (C=$N_{imthd.}$, and C=$C_{imthd.}$) 644, 695 (C–S). Elem. Anal. Calculated/Found: C: 53.69/53.64, H: 3.83/3.79, N: 12.52/12.47, S: 14.33/14.28, Ag: 12.05/12.00.

2.6 | Cell Culture

In this study, the highly metastatic, poorly differentiated, and aggressive non-small lung cancer (A549) cell line was used. The cells were cultured as monolayers in Dulbecco's Modified Eagle Medium (DMEM)-High Glucose supplemented with L-glutamine (Sigma Aldrich), non-essential amino acids (Multicell), sodium pyruvate (Multicell), 10% fetal bovine serum (FBS) (Gibco), and penicillin/streptomycin (Sartorius), in an incubator (ESCO) at 37°C with a 5% CO_2 atmosphere. Culture monitoring was performed using an inverted microscope (Zeiss).

2.7 | In Vitro Cytotoxicity Assay

The compounds we synthesized were treated at various concentrations, and their cytotoxic effects on A549 cells were determined using the commercially available MTT agent (Sigma Aldrich). For this purpose, cells were seeded into 96-well cell culture plates at a density of 1×10^4 cells/well. The following day, cells were treated with compounds prepared at specified concentrations (0.1, 0.5, 1, 5, 10, 50, 100 μM) and cultured for 72 h. At the end of this period, 10 μL/well MTT reagent (5 mg/mL) was added to each well and incubated for 4 h in culture conditions. Then, the formed insoluble formazan crystals were solubilized by dimethyl sulfoxide (100 μL/well). Subsequently, the absorbance of each well of a 96-well plate was measured at 570 nm with a 690 nm reference using a spectrophotometer (MultiscanGO, Thermo Fisher Sci.). Cell viability rates of the cells were calculated using the following formula.

Cell viability (%) : Abs of sample/Abs of control × 100.

2.8 | Molecular Docking Study

The structures of the ligands and complexes were built up with the help of Avogadro 1.2.060. Subsequently, the energy of the structures for the docking process was minimized using MMFF94 force field parameters within the Avogadro program [32]. The target structure for docking simulation was determined as PDB ID: 3UG2 [33]. The 3UG2 structure from the Protein Data Bank (PDB) represents the EGFR kinase domain with two mutations: G719S and T790M, bound to the inhibitor gefitinib. As it is well established, EGFR plays a critical role in cancer development, particularly in various types of carcinomas such as lung, breast, colon, and head and neck cancers [34–38]. Also, choosing 3UG2 for molecular docking studies in the context of NSCLC is significant since it has two key mutations on EGFR associated with NSCLC [33]. G719S mutation increases EGFR's kinase activity, leading to uncontrolled cell growth while The T790M mutation is responsible for acquired resistance in around 50%–60% of NSCLC patients treated with EGFR inhibitors. Therefore, the 3UG2 structure captures the dual mutation (G719S and T790M) in EGFR. In conclusion, 3UG2 is an excellent structure for studying the drug resistance mechanisms in NSCLC and for guiding the development of next-generation EGFR inhibitors.

Prior to molecular docking, all ions, ligands, and solvent molecules were removed from the 3UG2 target structure. Furthermore, any missing residues were incorporated into the 3UG2 structure in accordance with the data provided by the UniProt database [39], utilizing the CHARMM-GUI server [40]. Additionally, Kollman charges were incorporated for the protein residues, while Gasteiger charges were applied to the ligand. Subsequently, a docking method utilizing a Lamarckian genetic algorithm was employed to investigate the interactions between all ligands and gefitinib with the 3UG2 target structure, employing AutoDock 4.2.6 [41]. Furthermore, additional parameters for the silver atoms were incorporated for the molecular docking. 2D and 3D visualizations of the docking results were generated utilizing Discovery Studio [42]. 2D images of ligands and complexes except ligand **13** are given in Supporting Information (Figures S48–S53).

3 | Results and Discussion

3.1 | Chemical Evaluation of All Compounds

In this study, we used 5-amino-1,3,4-thiadiazole-2-thiol and reacted it with benzyl bromide in an ethanolic medium to produce a compound **(3)**. The resulting compound was then reacted with phenacyl bromide derivatives **(4a–4d)** to produce substituted 2-(benzylthio)-6-phenylimidazo[2,1-*b*][1,3,4] thiadiazole derivatives **(5–8)**. Subsequently, the Vilsmeier–Haack reagent was used to produce 2-(benzylthio)-6-phenylimidazo [2,1-*b*][1,3,4]thiadiazol-5-carbaldehyde derivatives **(9–12)** in the presence of phosphoryl chloride and *N*,*N*-dimethylformamide. Finally, in a 2:1 ratio, the resulting products were reacted with ethylenediamine in an ethanolic medium for 6 h to produce the targeted ligands **(13–16)**. The produced ligands were then reacted with silver acetate ($AgCH_3COO$) in a dimethyl sulfoxide medium to create the targeted complexes **(17–20)** (Scheme 1). For the characterization of the obtained compounds, melting point determination, FTIR, ^1H and ^{13}C NMR analysis, mass spectroscopy, and TGA were performed and confirmed the structure.

Magnetic susceptibility measurements of Ag(I) complexes obtained in the study were also made. As a result of the measurement, it was determined that all complexes were diamagnetic. According to these results, it is thought that all complexes may be in either triangular bipyramid or square pyramidal geometry with sp^3d hybridization in d^{10} electronic configuration.

3.2 | FTIR Evaluation of the Ligands and Complexes

FTIR spectroscopy analysis was carried out for the determination and characterization of the ligand and complexes functional groups. The stretching bands observed at 3278 cm^{-1} for NH_2, 3098 cm^{-1} for aromatic C–H, 1641 cm^{-1} for thiadiazole C=N, and 694 cm^{-1} for C–S in the FTIR spectrum are evidence for the successful synthesis of the starting compound **3** [43]. When evaluating **5–8** compounds, resulting from the reaction of compound (**3**) and phenacyl bromide derivatives **4(a–d)**, we figured out that the stretching bands at the range of 3028–3048 cm^{-1} for aromatic C–H, at the range of 1598–1612 cm^{-1} for imidazothiadiazole C=N, at the range of 1022–1087 cm^{-1} for N–N, and the range of 691–695 cm^{-1} for C–S groups [33, 44]. In the same way, when we evaluated the FTIR spectra of the **(9–12)** compounds, resulting from the carbonylation reaction of compounds **(5–8)**, we concluded that the stretching bands were observed at the range of 3006–6058 cm^{-1} for aromatic C–H, 1654–1674 cm^{-1} for C=O, 1054–1092 cm^{-1} for N–N, and 695–691 cm^{-1} for C–S groups [33, 44]. Evaluation of FTIR spectra of the targeted ligands resulted from the reaction of compounds **(9–12)** and ethylenediamine concluded the disappearance of C=O peaks and appearance of imine (C=N) stretching bands at 1626, 1625, 1622, and 1644 for ligands **(13–16)**, respectively, is strong evidence for the successful synthesizing of these ligands [45]. The shift of the C=N peak for the azomethine group from the range of 1622–1644 cm^{-1} for the ligands to the range of 1640–1644 cm^{-1} for the complexes **(17–20)** is evidence for the formation of the Ag(I) complexes (Figure 1). The observation of C=O stretching bands in the range of 1668–1681 cm^{-1} in complex compounds also showed that acetate groups were coordinated to the silver nucleus. Below is the FTIR spectra for the complex **17** while the rest of the spectrum is attached to the Supporting Information (Figures S1–S17).

3.3 | Evaluation of ^1H and ^{13}C NMR Spectra

^1H and ^{13}C NMR spectroscopy analysis were carried out for the determination and characterization of the compound's functional group position. The signals at the range of 7.37–7.36 ppm for $CH_{ar.}$ protons, 7.32 ppm for NH_2, and 4.30 ppm for SCH_2

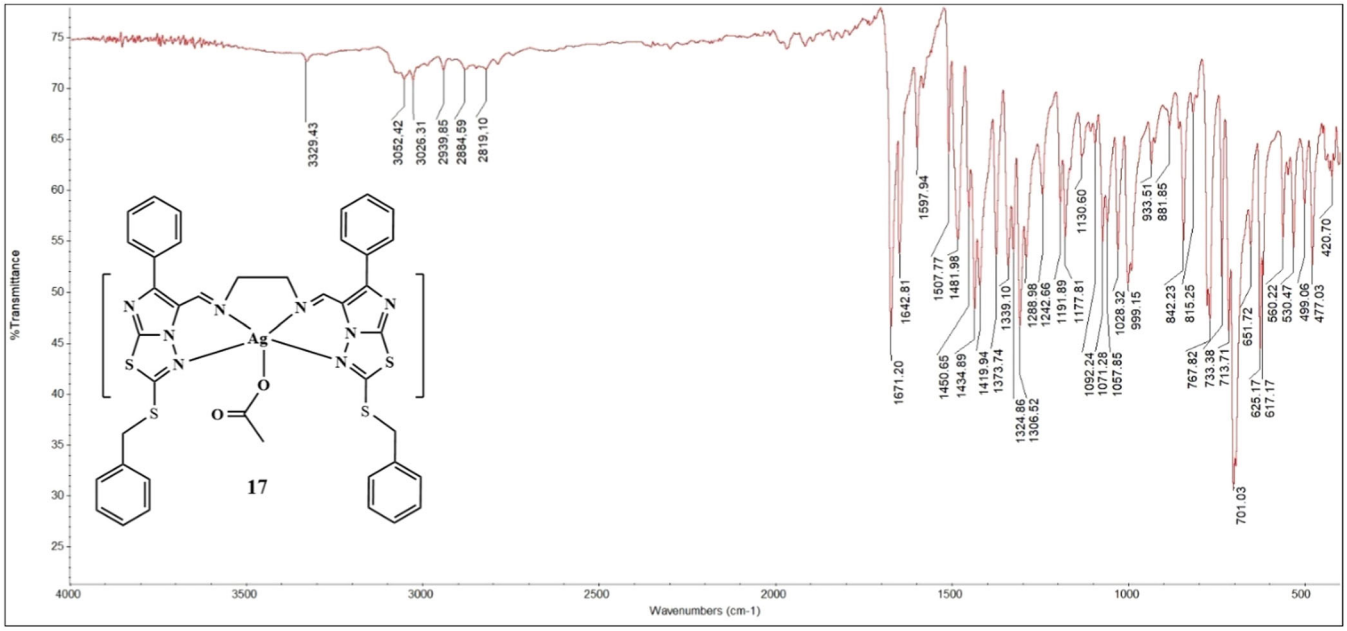

FIGURE 1 | FTIR spectra of complex **17**.

protons in ^{1}H NMR spectrum. The signals at 170.34 ppm of C–NH_2 atoms for thiadiazole ring, 149.97 ppm for C=N, 137.57, 129.45, 128.95, 127.91 ppm for C–$C_{ar.}$, and 38.94 ppm for C–S in ^{13}C NMR spectrum are evidence for successfully synthesizing of starting compound **(3)** (Figures S18 and S19) [4].

^{1}H NMR signals at the range of 7.95–7.87 ppm for imidazothiadiazole ring, at the range of 7.80–6.95 ppm for aromatic C–H, and at the range of 4.44 4.45 ppm for S–CH_2, while signals at 2.38 ppm for CH_3, and 3.84 ppm for OCH_3, and ^{13}C NMR signals at the range of 159.53–158.88 ppm, and the range of 146.09–144.88 ppm for imidazothiadiazole groups, at the range of 137.40–124.93 ppm for aromatic carbons, at 55.33 ppm for OCH_3 group, at the range of 38.81–38.73 ppm for S–CH_2 groups, and at 21.26 ppm for CH_3 group are strong evidence for the formation of targeted compounds **(5–8)** (Figures S20–S27) [46].

The disappearance of signals at the range of 7.95–7.87 ppm for the carbon number 5 at the imidazothiadiazole ring and appearance of signals at the range of 10.07–10.03 ppm for O=CH, and observing of signals at 7.86–7.02 ppm for C–$H_{ar.}$, 4.55–4.54 ppm for SCH_2, 3.86 ppm for OCH_3, and 2.42 ppm for CH_3, and ^{13}C NMR signals at the range of 177.37–177.01 ppm for carbonyl carbons, 162.75–161.04 ppm and 155.81–150.25 ppm for imidazothiadiazole groups, 140.07–123.71 ppm for aromatic carbons, at 55.41 ppm for OCH_3 group, 38.69–38.63 ppm for S–CH_2 groups, and 21.42 ppm for CH_3 group are evidence for successfully synthesizing of compounds **(9–12)** (Figures S28–S35) [47, 48].

In the ^{1}H NMR spectrum of the synthesized ligands, we observed disappearance of signals at 10.07–10.03 ppm for O=CH, and appearance of singlet signals at 8.47–8.41 ppm corresponds to N=CH, doublet signals at 7.87–6.75 ppm corresponds to aromatic C–H, singlet signals at 4.49–4.29 ppm corresponds to S–CH_2 and singlet signals at 4.06–4.04 ppm corresponds to N–CH_2 are strong evidence for the formation of ligands (**13–16**). Singlet signals at 2.27 ppm for CH_3 and 3.71 ppm for OCH_3 are for the ligands **15** and **16**, respectively. While the study of ^{13}C NMR revealed that, carbonyl carbon signals disappeared, and signals at 160.29–159.69 ppm for imidazothiadiazole C=N, 150.56–148 ppm for imine C=N, 149.12–146.34 ppm for imidazothiadiazole C=C, 130.78–112.90 ppm for aromatic C–H are another evidence for the synthesis of the targeted ligands. Below are the ^{1}H and ^{13}C NMR spectra for the ligand **13** (Figures 2 and 3), while the rest of the spectra are attached to the Supporting Information (Figures S36–S41) [49].

3.4 | Evaluation of Electrospray Ionization Mass Spectrometry (ESI-MS) Data of All Ligands and Complexes

Electrospray ionization mass spectrometry (ESI-MS) confirmed the successful synthesis of the ligands. The experimental M/Z values for **13–16** were 727.20 (35%), 819.18 (100% M^{+}+Na), 755.27 (38%), 787.26 (64%), respectively; while it was 892.10 (37%), 959 (62%), 920 (72%), 952 (53%) for **17–20**, respectively, which agreed well with their calculated molecular weights. Below are the ESI-MS spectra for the ligand **13** and complex **17** (Figures 4 and 5), while the rest of the spectra are attached to the Supporting Information (Figures S42–S47).

3.5 | Evaluation of Thermogravimetric Analysis

In this study, the thermal decomposition behavior and the substituted functional groups of Ag(I) complexes with selected ligands (**13** and **15**) specifically **17**, and **19** were investigated. TGA and differential thermal analysis (DTA) were performed in a controlled nitrogen (N_2) environment at a heating rate of 10°C/min, spanning from 25°C to 800°C. Prior to analysis, all samples were dried under vacuum at 60°C for 4 h.

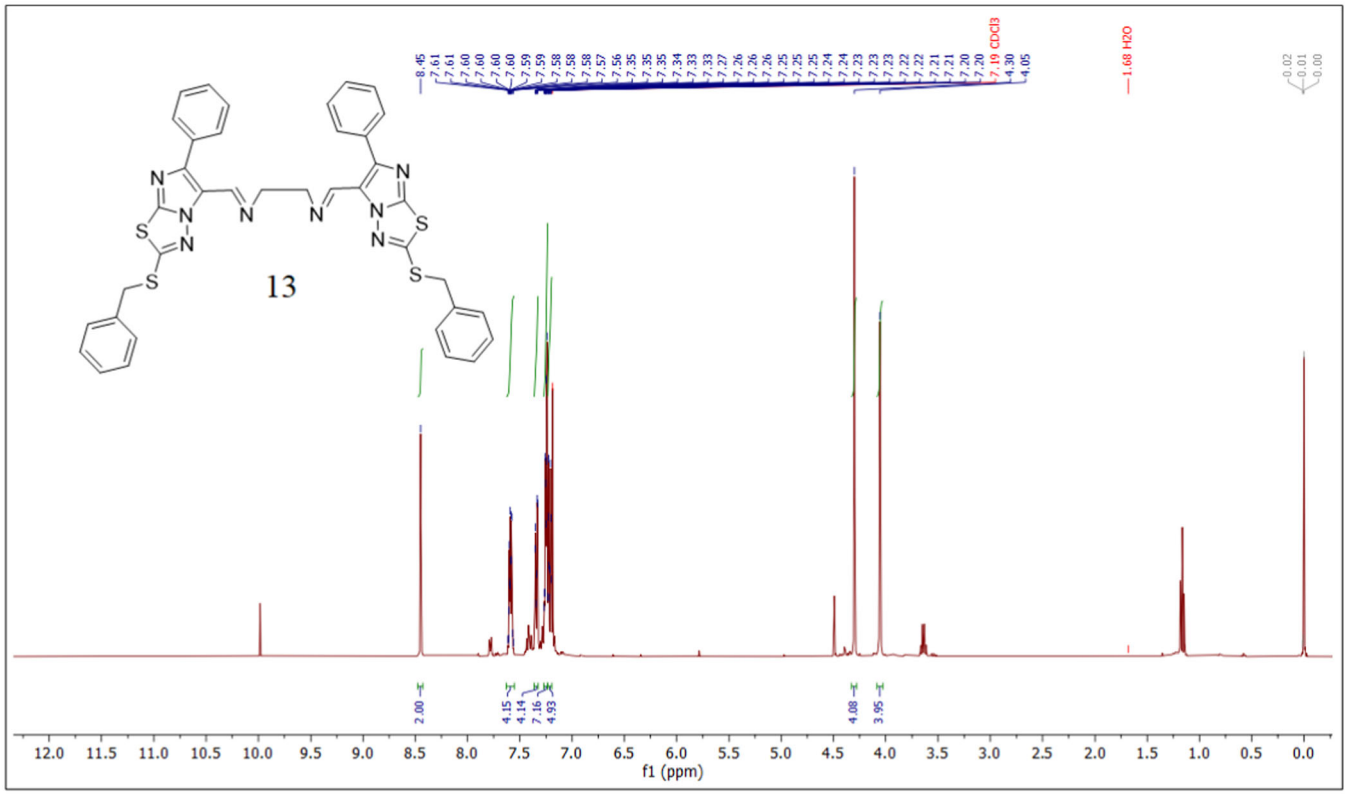

FIGURE 2 | ^{1}H NMR spectrum of the ligand **13**.

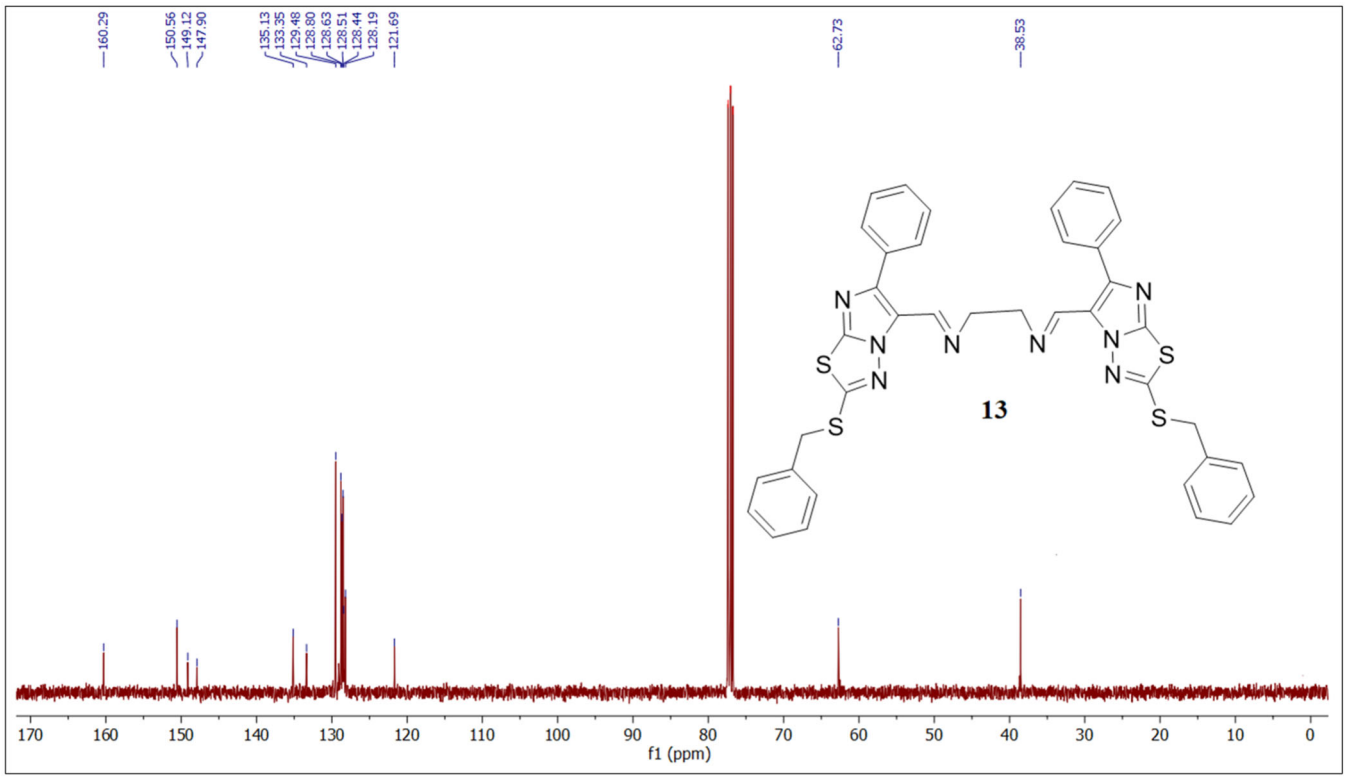

FIGURE 3 | ^{13}C NMR spectrum of the ligand **13**.

Upon examination of the TGA curve of complex **17**, degradation is observed to occur in two distinct steps (Figure 6). The first decomposition step takes place between 175°C and 380°C, resulting in a mass reduction of 34.00%. This observed reduction closely matches the theoretical mass reduction of 34.17%. This agreement between calculated and measured values corresponds to the separation of the Ar–CH_2–S and CH_3COO– groups from the main molecule. The second

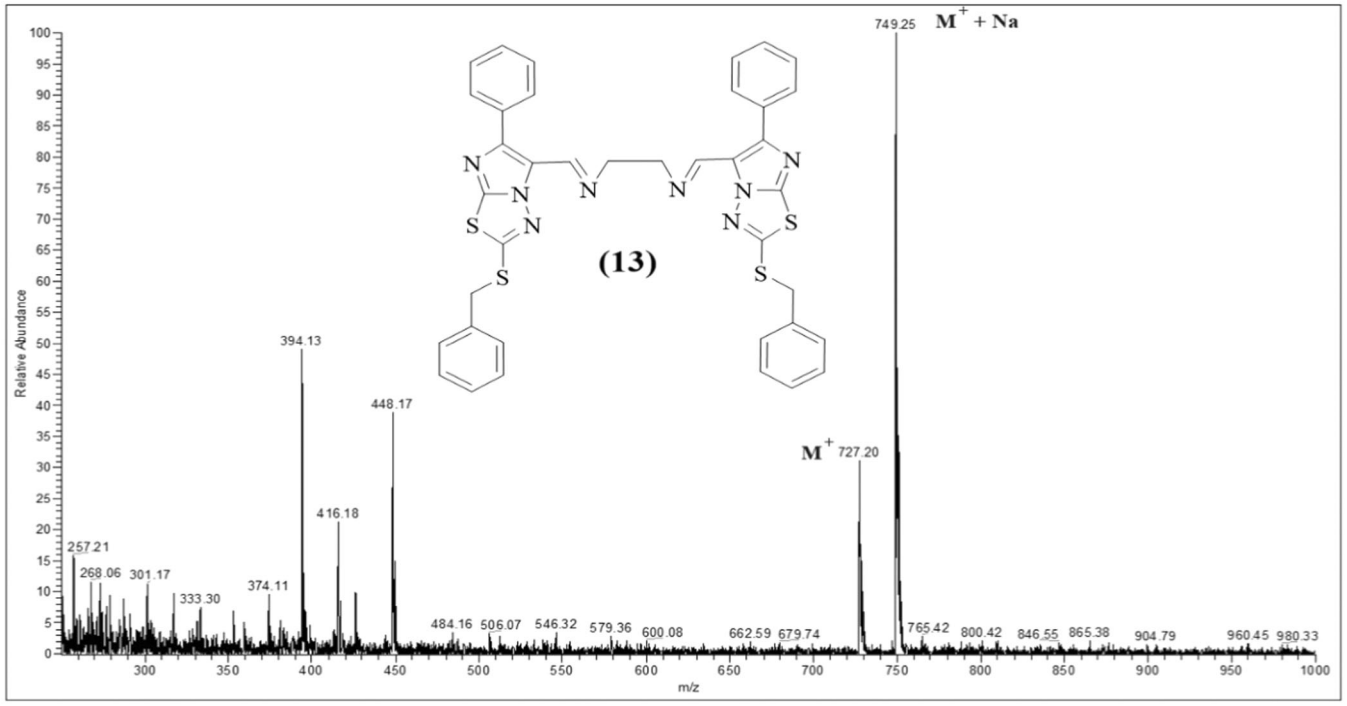

FIGURE 4 | ESI-MS spectrum of ligand **13**.

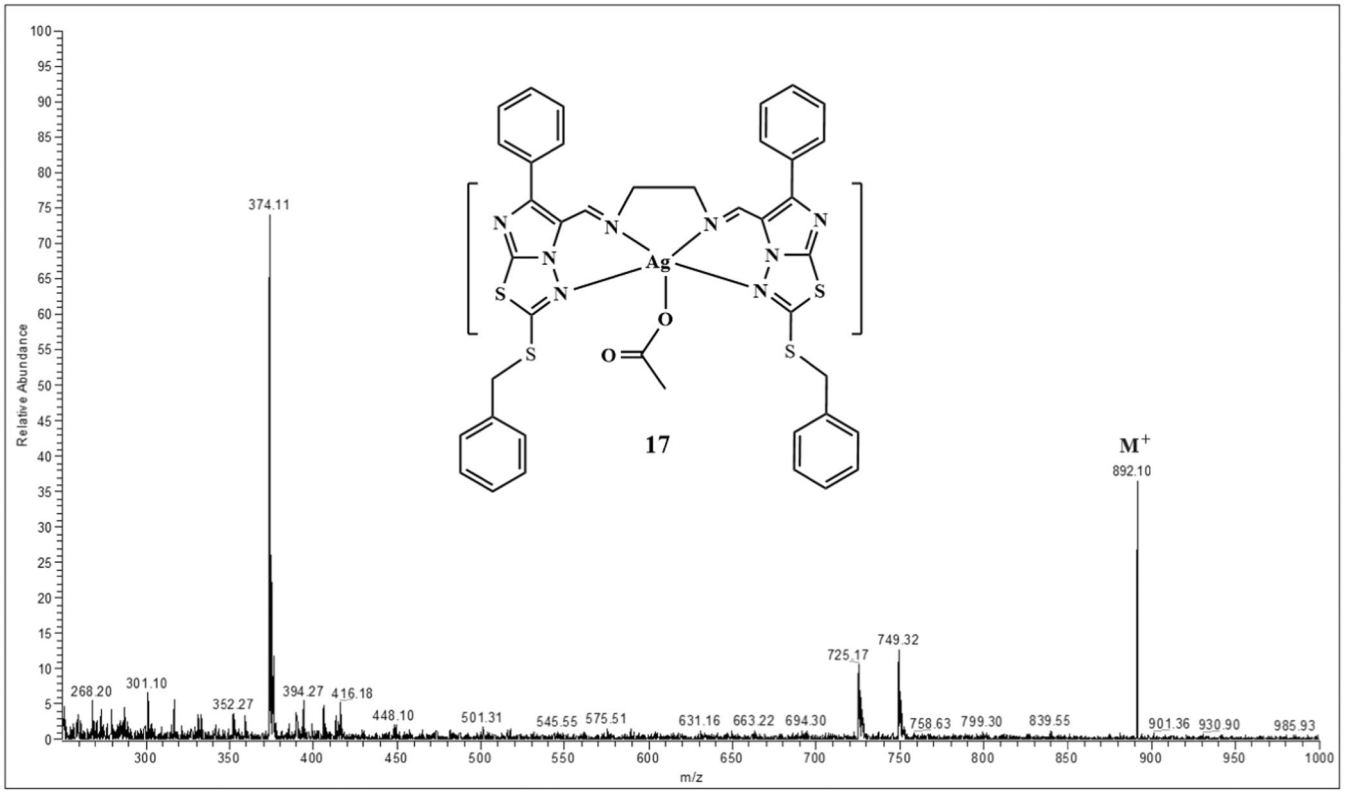

FIGURE 5 | ESI-MS spectrum of complex **17**.

degradation step occurs between 380°C and 610°C, with a mass reduction of 42.99%, which is attributed to the remaining organic structure. No further weight loss is observed after this temperature, as the TGA analysis was terminated at 800°C. These results demonstrate a strong correlation between the computed values and empirical observations, thus supporting the proposed structure of the target complex.

Upon examining the TGA curve of complex **19**, it is observed that degradation occurs in two steps (Figure 7). The first decomposition step takes place between 180°C and 350°C, with

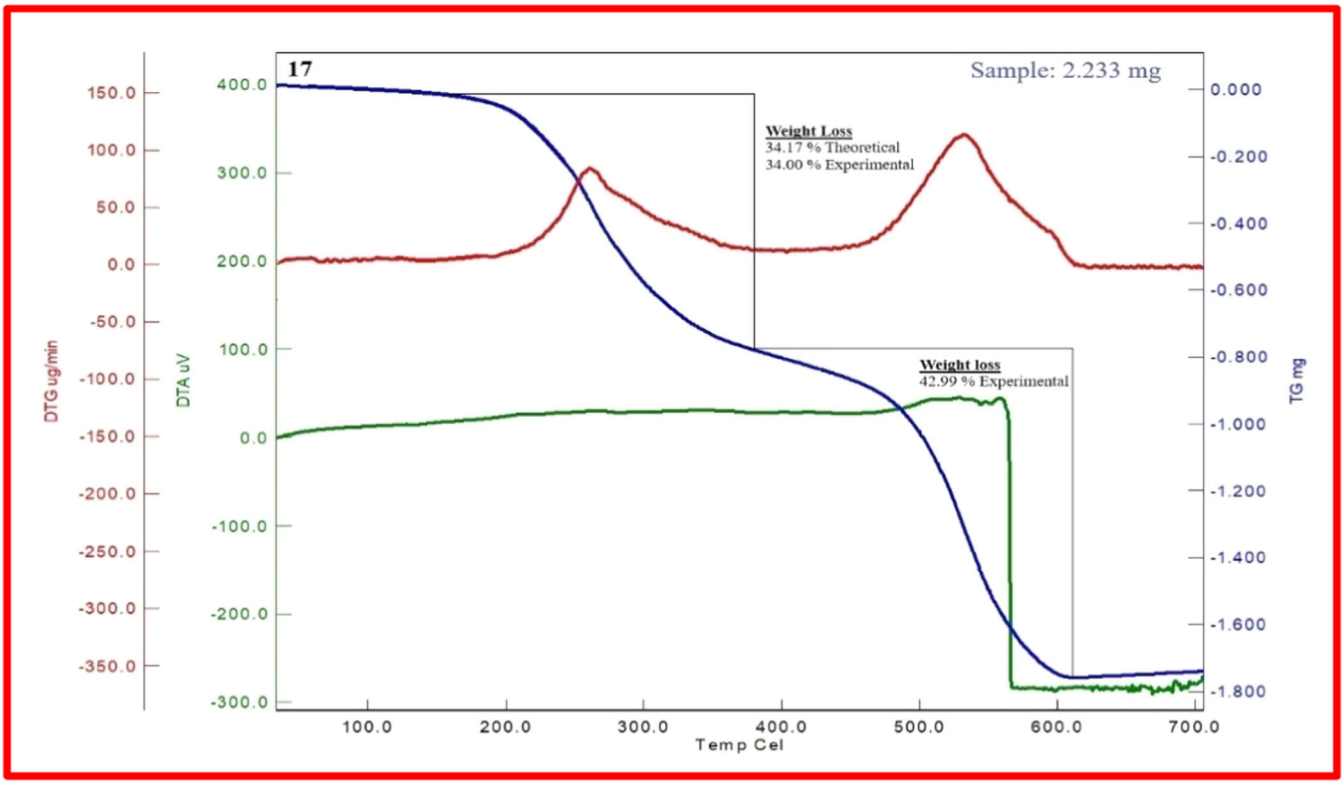

FIGURE 6 | TGA–DTG/DTA curve of complex **17**.

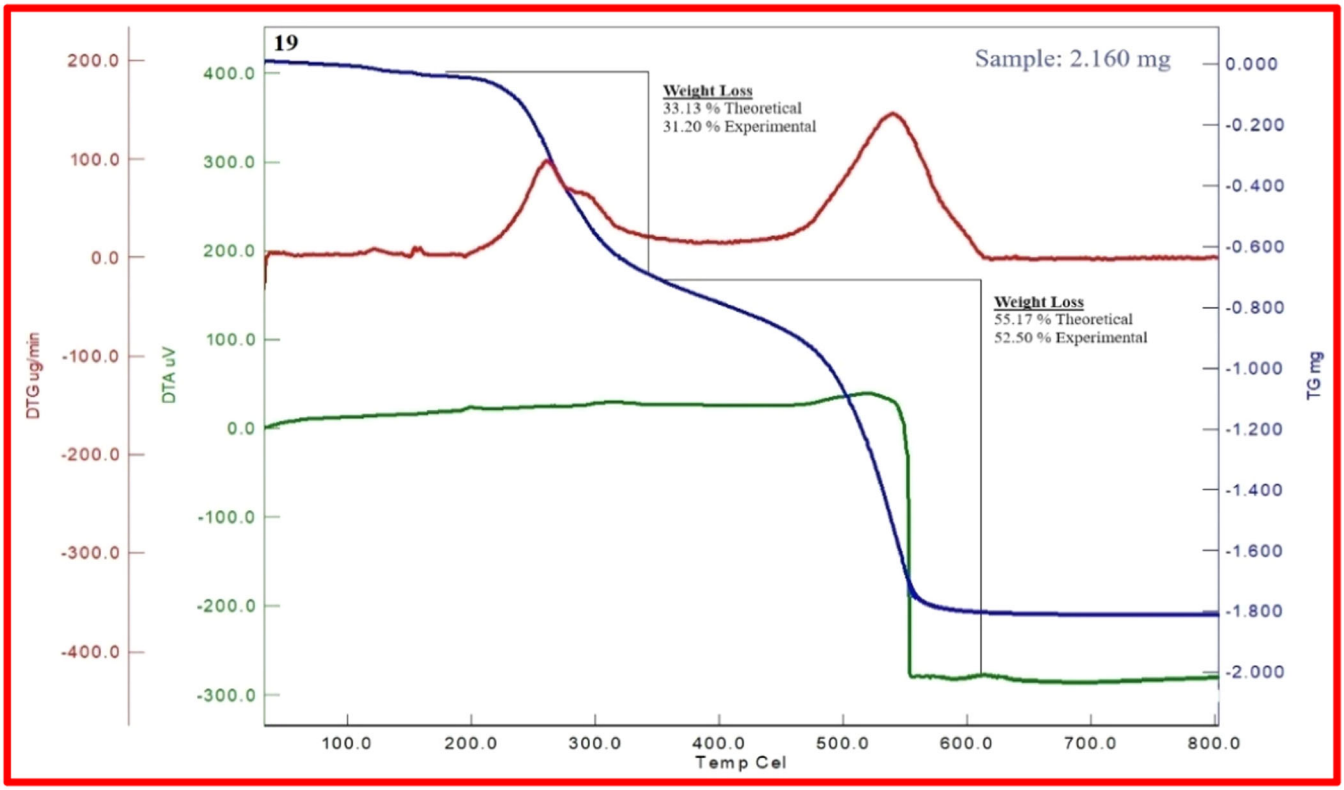

FIGURE 7 | TGA–DTG/DTA curve of complex **19**.

a mass reduction of 31.20%. The calculated theoretical mass reduction for this step is 33.13%. Both the calculated and measured mass reductions correspond to the loss of the Ar–CH_2–S and CH_3COO– groups from the main molecule. The second degradation step occurs between 350°C and 610°C, resulting in a mass reduction of 52.50%, which corresponds to the remainder of the organic structure. The calculated theoretical mass reduction for this step is 55.17%. No additional

weight loss is observed after this temperature due to the termination of the TGA analysis at 800°C. These results demonstrate a strong correlation between the calculated values and empirical observations, thereby supporting the proposed structure of our target complex.

3.6 | In Vitro Investigation, Molecular Docking Evaluation, and Cytotoxicity Effect of the Synthesized Ligands and Complexes

3.6.1 | In Vitro Cytotoxic Effects of Compounds on Nonsmall Lung Cancer Cell Line

This study comprehensively analyzes the cytotoxic effects of various compounds on A549 lung cancer cells. The findings underscore the potential of certain compounds and their silver complex as potent cytotoxic agents, warranting further research into their mechanisms of action and potential therapeutic applications.

Ligand **13** exhibits a robust dose-dependent cytotoxic effect, with cell viability plummeting to 15.2% at 25 μg/mL and fully cytotoxic at 50 μg/mL and above. This significant reduction suggests a high potency of ligand **13** against A549 cells, making it a strong candidate for further investigation. Complex **17** also shows dose-dependent cytotoxicity, though it is less potent compared to ligand **13**. Despite this, it still demonstrates notable activity with a viability of 54.19% at 25 μg/mL, 33.61% at 50 μg/mL, and fully cytotoxic at 100 μg/mL, indicating that the silver complex may enhance the efficacy of the base compound. According to these results, ligand **13** was found to have ~3.56-fold higher cytotoxic effect at 25 μg/mL and 10-fold higher cytotoxic effect at 50 μg/mL concentration than its Ag complex.

Ligand **14** shows minimal cytotoxicity with cell viability remaining high (around 90% even at 100 μg/mL). This suggests that ligand **14** is relatively ineffective against A549 cells. Complex **18** displays a similar low potency, with slight decreases in cell viability but still maintaining viabilities above 87% at all tested concentrations. The presence of silver does not appear to significantly enhance the activity of ligand **14**.

Ligand **15** demonstrates moderate cytotoxicity, with a viability of 64.98% at 100 μg/mL. This indicates that ligand **15** has potential but is not as potent as some other compounds. Complex **19** exhibits higher efficacy with a reduced viability of 35.07% at 100 μM, highlighting the potential enhancement of activity by the silver complex.

Ligand **16** shows moderate cytotoxic effects, with viability decreasing to 56.34% at 100 μM. This suggests moderate potential for ligand **16**. Complex **20** demonstrates greater potency, reducing viability to 27.02% at 100 μM. The silver complex significantly enhances the cytotoxic effect of ligand **16**. At concentrations of 50 μg/mL and above, the complex **20** has 1.3–2.1-fold higher cytotoxicity than ligand **16** on A549 cells (Table 1).

According to the current drug sensitivity reports in cancer of Sanger Institute and Massachusetts Cancer Center (www.cancerrxgene.org), IC_{50} values for cisplatin and etoposide, which are frequently used chemotherapeutics in the treatment of A549 cells, were determined as 20.23 and 0.95 μM, respectively. Another important class of agents used in the treatment of NSCLC is receptor tyrosine kinase inhibitors (TKIs). Among these, gefitinib is a commonly utilized EGFR inhibitor. The EGFR is overexpressed in the majority of NSCLC cells [49]. The use of neutralizing antibodies against EGFR was the most widely accepted third-line treatment regimen. However, the discovery of activating mutations in this receptor led the medical community to support the use of TKIs of EGFR. Gefitinib was the first TKI developed against EGFR. Clinical studies have shown significant differences in response to TKIs. There were significant responses in patients with G719X and L858R mutations. More importantly, patients with mutations in exons 18–21 other than these two mutations respond very poorly to TKIs. This has changed the way patients with NSCLC are treated. The original rationale for using TKIs was based on EGFR expression levels. However, in the presence of certain mutations, the response to TKI therapy may not be acceptable [50]. Gefitinib is selective inhibitor for EGFR activation via binding to ATP-competitive binding sites and is used for targeted therapy. However, lung cancer cells are capable of developing resistance to gefitinib therapy [51]. For example, the T790M mutation identified in EGFR exon 19 causes resistance

TABLE 1 | Cell viability rates according to the concentration of the synthesized compounds in A549 cell line.

	Cell viability (%)					
		Conc.				
Compound	**Control**	**6 μg/mL**	**12 μg/mL**	**25 μg/mL**	**50 μg/mL**	**100 μg/mL**
13	100 ± 15.2	47.91 ± 3.2	23.45 ± 1.5	15.22 ± 1.8	3.35 ± 0.3	3.67 ± 0.3
17	100 ± 12.7	77.02 ± 4.9	62.03 ± 5.6	54.18	33.61 ± 6	7.01 ± 2.2
14	100 ± 3.4	94.59 ± 2.7	94.74 ± 2.5	96.23 ± 3.8	93.72 ± 2.2	90.68 ± 6.9
18	100 ± 8.7	92.17 ± 8.7	94.24 ± 5.1	91.28 ± 8.9	92.33 ± 11.9	87.69 ± 6.2
15	100 ± 8.9	97.19 ± 8.3	99.74 ± 4.8	96.85 ± 16.9	74.58 ± 10.4	64.98 ± 6.1
19	100 ± 3.8	95.32 ± 3	96.73 ± 4.5	80.58 ± 8.2	49.15 ± 4.5	35.07 ± 1
16	100 ± 4.8	97.39 ± 5	98.89 ± 9	88.25 ± 6.8	70.81 ± 3.2	56.34 ± 5.8
20	100 ± 0.66	97.88 ± 2	98.28 ± 6.5	79.56 ± 6.8	54.52 ± 6.3	27.02 ± 3.2

TABLE 2 | Average IC_{50} values of the synthesized compounds and gefitinib in A549 cell line.

Compounds	13	17	14	18	15	19	16	20	Gefitinib
IC_{50} (μg/mL)	5.43	23.11	470.25	437.12	144.53	56.81	113.60	55.21	3.76

to EGFR-TKI agents [52]. In this respect, the EGFR mutation spectrum determines the response to gefitinib treatment. According to the literature of gefitinib-induced growth inhibition, the IC_{50} value of gefitinib in A549 cells was calculated to be 8.42 μM (3.76 μg/mL) (Table 2) [52]. Besides that, gefitinib inhibits tumor progression, metastasis, angiogenesis, and also induces autophagy and apoptosis in A549 cells through the PI3K/AKT/mTOR pathway [51]. According to this evidence, among the newly synthesized compounds in this study, the one with similar cytotoxicity to gefitinib is compound **13** (Table 2). In light of the literature, there is a need for alternative combined treatment strategies for resistant NSCLC to chemotherapeutic agents and TKI molecules. In this context, we believe that compound **13** is a valuable molecule that can be considered in further research as a candidate molecule in the treatment of gefitinib-resistant lung cancer cells.

According to our data, it can be said that ligand **13** has promising strong cytotoxic effects with the lowest IC_{50} value (5.43 μg/mL) among other compounds. In addition to this, the newly synthesized complexes **17**, **19**, and **20** (IC_{50} values; 23.11, 56.81, and 55.21 μg/mL, respectively) may also be suggested to have possible potential anticancer effects (Table 2).

3.6.2 | Molecular Docking Evaluation

The docking binding scores allow for a comparative analysis of their binding affinity and inhibitory efficacy against EGFR. In this context, according to the performed docking simulation the binding affinities of the synthesized compounds and Gefitinib, reference drug for 3UG2, from strongest to weakest, are as follows: **13**, gefitinib (−9.8 kcal/mol) > **17** (−9.7 kcal/mol) > **19**, **20** (−9.5 kcal/mol) > **15**, **16** (−9.2 kcal/mol) > **18** (9.0 kcal/mol) > **14** (8.9 kcal/mol) > gefitinib (−8.9 kcal/mol). The binding scores of compounds, expressed as negative values, indicate binding strength and range from −8.8 to −9.8 kcal/mol. Compound **13** shows the highest binding affinity with a score of −9.8 kcal/mol, indicating it binds most effectively to EGFR among the tested compounds (Figure 8). Other compounds with strong binding scores include complexes **17**, **19**, and **20**, ranging from −9.7 to −9.5 kcal/mol. On the other hand, the reference compound, gefitinib, has a binding affinity of −9.8 kcal/mol. Accordingly, gefitinib and compound **13** display both high binding affinities (−9.8 kcal/mol) and low IC_{50} values (3.76 and 5.43 μM, respectively), suggesting that strong binding correlates well with potent inhibition. This alignment confirms that gefitinib and compound **13** are likely to be highly effective against EGFR. Also, complexes **17**, **19**, and **20** also show a reasonable correlation between docking scores (−9.7, −9.5, and −9.5 kcal/mol) and moderate IC_{50} values (23.11, 56.81, and 55.21 μM), suggesting that binding affinity contributes to their biological potency. In summary, docking scores and IC_{50} values correlate well for compounds **13**, **17**, **19**, and **20**, indicating that binding affinity contributes to their in vitro efficacy. Also, compound **13**, with the strongest results in both metrics, is the most promising candidate for further investigation. In this regard, we furthermore displayed the 2D interaction diagram and 3D binding pose of compound **13** to EGFR (Figure 8). Accordingly, the 2D docking interaction results between compound **13** and EGFR reveal various noncovalent bonds that play a crucial role in stabilizing the molecular complex and influencing biological activity. A more in-depth discussion shows that compound **13** exhibits a total of three pi–sulfur interactions, one with the MET790 residue of EGFR and two with the CYS797 residue of EGFR. Here, the interaction of the MET790-mutated residue in the 3UG2 EGFR structure with compound **13** may hold significant implications for NSCLC treatment. The MET790 mutation in EGFR is associated with acquired resistance to EGFR inhibitors in NSCLC, such as gefitinib and erlotinib, which are common treatments. This mutation alters the binding site conformation, often reducing the efficacy of first-generation TKIs by blocking or weakening their interactions. Hence, pi–sulfur interaction of the ligand **13** with MET790 can be crucial because it strengthens ligand binding, particularly when the mutation alters the local electron distribution around MET790, which may enhance the ligand's anchoring to the mutated site. Accordingly, it can be said that such interactions can potentially counteract the destabilizing effects of the mutation, allowing the ligand to bind effectively even with the presence of MET790 mutations, which could otherwise lead to drug resistance. Also, it is well known that these pi-sulfur bonds are formed between the electron clouds of sulfur-containing amino acids and the aromatic rings of the ligand, stabilizing the ligand's binding position. Hence, it can be stated that these interactions facilitate binding of ligands within the active site of EGFR. Also, two pi–pi stacked interactions with PHE723 occur through the stacking of aromatic rings, which contributes to the stability of the ligand within the binding site. On the other hand, residues such as ALA743, VAL726, MET790, LYS745, LEU718, and LEU844 participate in alkyl and pi–alkyl interactions, further stabilizing the ligand's position within the hydrophobic region of EGFR. Also, it is well established that these hydrophobic interactions occur through Van der Waals forces, preventing the ligand from dislocating from its binding site and supporting sustained interaction with the target protein. In summary, the mentioned interactions collectively enhance the binding and inhibitory potential of the ligand toward EGFR. The density of pi–sulfur and hydrophobic interactions strengthens the ligand's position in the binding site, potentially enabling effective inhibition of EGFR's biological activity. Below is the 2D interaction diagram between ligand **13** and 3UG2 (Figure 8), while the other diagrams are attached to the Supporting Information (Figures S48–S53).

4 | Conclusion

In this work, four novel Schiff bases containing 2,5,6-trisubstituted imidazothiadiazole derivatives ligands **(13–16)**

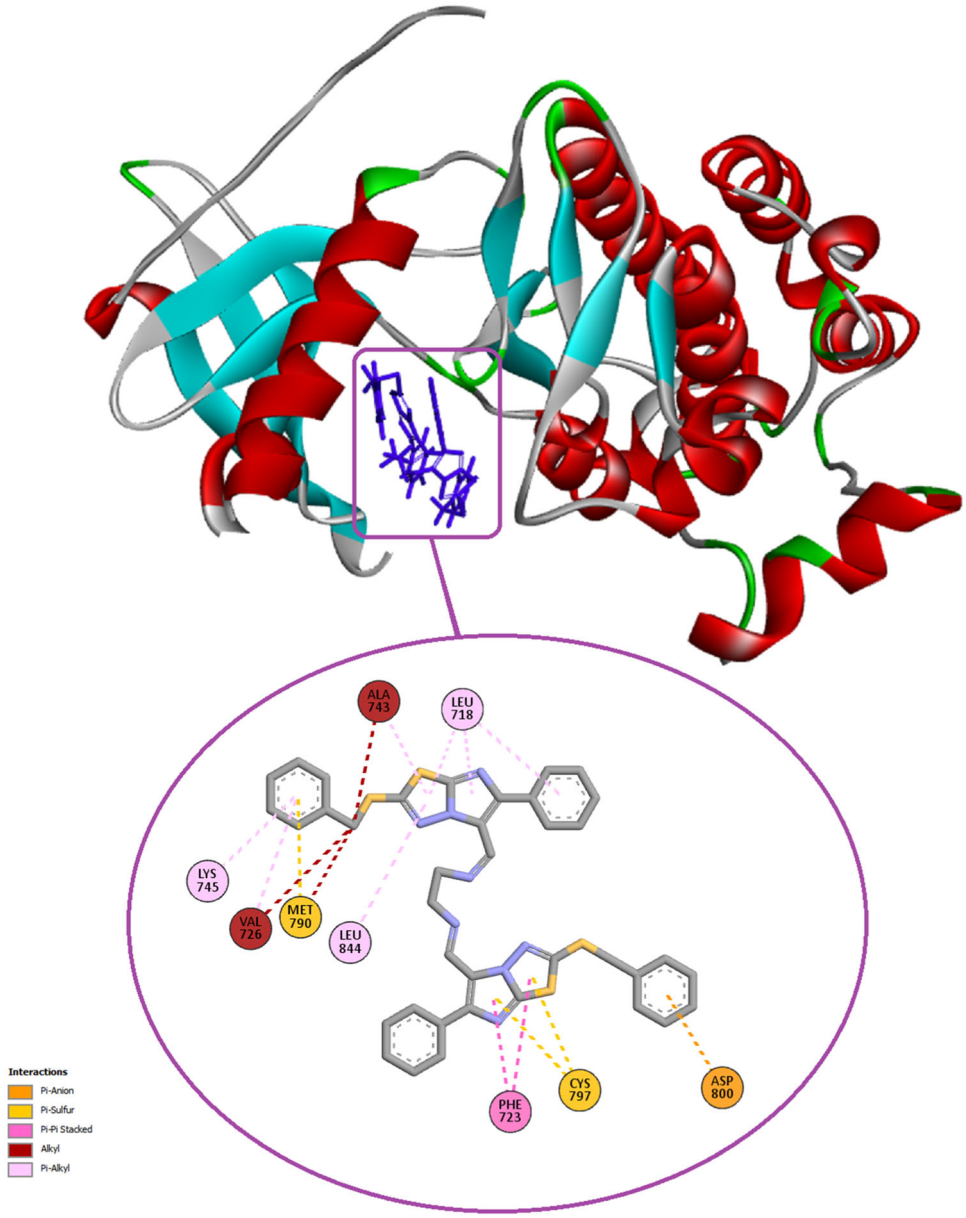

FIGURE 8 | 2D interaction diagram and 3D binding pose of the compound **13** to 3UG2.

were conveniently synthesized and meticulously characterized through the application of elemental analysis, ^{1}H and ^{13}C NMR spectroscopy, FTIR spectroscopy, ESI-MS spectroscopy, and TGA methods. The Ag(I) complexes of these ligands were synthesized in dimethylsulfoxide media. Their structures were characterized using FTIR spectroscopy and TGA. The metal contents in all complexes were analyzed using ICP-OES spectroscopy. The thermal stabilities of some complexes were determined using TGA. It was understood that the resulting complexes showed high thermal stability.

Cytotoxic activity tests indicate varying levels of cytotoxicity among the tested compounds and their silver complexes. The potency of the silver complexes Ag(I) generally appears higher than their parent compounds, suggesting the silver form may enhance the cytotoxic properties. Ligands **13**, **15**, and **16** along with their silver complexes, demonstrate particularly strong cytotoxic effects, making them potential candidates for further investigation as anticancer agents. The variations in cytotoxicity highlight the importance of structural modifications in drug development. Also, the molecular docking results demonstrated a strong correlation between the high binding affinities against of certain compounds and their observed in vitro biological activity. Molecular docking studies further demonstrated that ligand **13**, in particular, binds with high affinity to the EGFR, stabilizing effectively in the presence of the MET790 mutation, a mutation associated with drug resistance in NSCLC. These interactions suggest a mechanism through which ligand **13** can counteract resistance-related conformational changes, thereby enhancing its inhibitory efficacy.

These findings highlight the potential of certain silver complexes as more effective anticancer agents and underscore the need for further investigation into their mechanisms of action and therapeutic potential. Further studies are warranted to elucidate the mechanisms underlying these effects and to explore the potential of these compounds and their complexes in cancer therapy.

Author Contributions

Ahmed Hamdi Mirghani: resources, methodology, investigation, formal analysis, writing–original draft. **Suray Pehlivanoglu:** investigation, resources, cytotoxic activity testing. **Hakan Alici:** investigation, theoretical calculations. **Hakan Tahtaci:** investigation. **Saban Uysal:** writing–review and editing, validation, supervision, investigation, formal analysis, funding acquisition.

Acknowledgments

We would like to thank the KBU-BAP unit for supporting this study with BAP project no: KBUBAP-23-DR-018.

Conflicts of Interest

The authors declare no conflicts of interest.

Data Availability Statement

Data will be made available on request.

References

1. P. A. Datar and T. A. Deokule, "Design and Synthesis of Thiadiazole Derivatives as Antidiabetic Agents," *Medicinal Chemistry* 4 (2014): 390–399, https://doi.org/10.4172/2161-0444.1000170.

2. A. K. Jain, S. Sharma, A. Vaidya, V. Ravichandran, and R. K. Agrawal, "1,3,4-Thiadiazole and Its Derivatives: A Review on Recent Progress in Biological Activities," *Chemical Biology & Drug Design* 81 (2013): 557–576, https://doi.org/10.1111/cbdd.12125.

3. E. E. Oruç, S. Rollas, F. Kandemirli, N. Shvets, and A. S. Dimoglo, "1,3,4-Thiadiazole Derivatives. Synthesis, Structure Elucidation, and Structure−Antituberculosis Activity Relationship Investigation," *Journal of Medicinal Chemistry* 47 (2004): 6760–6767, https://doi.org/10.1021/jm0495632.

4. M. Erdogan, K. Kiymaz, H. Tahtaci, and S. Uysal, "Synthesis and Characterization of the Co(II) and Ni(II) Complexes of 1,3,4-Thiadiazole-Derived Ketones and Secondary Alcohols: Thermal and Magnetic Properties," *Journal of Coordination Chemistry* 74 (2021): 2508–2533, https://doi.org/10.1080/00958972.2021.1992401.

5. H. Bhuva, D. Sahu, B. N. Shah, D. C. Modi, and M. B. Patel, "Biological Profile of Thiadiazole," *Pharmacologyonline* 1 (2011): 528–543.

6. J. J. Li, *Name Reactions in Heterocyclic Chemistry* (Canada: John Wiley & Sons, 2004), https://doi.org/10.1002/0471704156.

7. M. Er, A. Özer, Ş. Direkel, T. Karakurt, and H. Tahtaci, "Novel Substituted Benzothiazole and Imidazo[2,1-b][1,3,4]thiadiazole Derivatives: Synthesis, Characterization, Molecular Docking Study, and Investigation of Their In Vitro Antileishmanial and Antibacterial Activities," *Journal of Molecular Structure* 1194 (2019): 284–296, https://doi.org/10.1016/j.molstruc.2019.05.104.

8. E. B. Lindgren, M. A. de Brito, T. R. A. Vasconcelos, et al., "Synthesis and Anticancer Activity of (E)-2-Benzothiazole Hydrazones," *European Journal of Medicinal Chemistry* 86 (2014): 12–16, https://doi.org/10.1016/j.ejmech.2014.08.039.

9. M. Er, F. Ahmadov, T. Karakurt, Ş. Direkel, and H. Tahtaci, "A Novel Class Substituted Imidazo[2,1-b][1, 3, 4]thiadiazole Derivatives: Synthesis, Characterization, In Vitro Biological Activity, and Potential Inhibitors Design Studies," *ChemistrySelect* 4 (2019): 14281–14290, https://doi.org/10.1002/slct.201903886.

10. H. Tahtaci and G. Aydın, "A Simple and Efficient Approach for the Synthesis of a Novel Class Aliphatic 1,3,4-Thiadiazol-2 (3H)-one Derivatives via Intramolecular Nucleophilic Substitution Reaction," *Synthetic Communications* 49 (2019): 2357–2368, https://doi.org/10.1080/00397911.2019.1623257.

11. H. Tahtaci, H. Karacık, A. Ece, M. Er, and M. G. Şeker, "Design, Synthesis, SAR and Molecular Modeling Studies of Novel Imidazo[2, 1-b][1, 3, 4]thiadiazole Derivatives as Highly Potent Antimicrobial Agents,," *Molecular Informatics* 37 (2018): 1700083, https://doi.org/10.1002/minf.201700083.

12. P. Niu, J. Kang, X. Tian, et al., "Synthesis of 2-Amino-1,3,4-oxadiazoles and 2-Amino-1,3,4-thiadiazoles via Sequential Condensation and I_2-Mediated Oxidative C–O/C–S Bond Formation," *Journal of Organic Chemistry* 80 (2015): 1018–1024, https://doi.org/10.1021/jo502518c.

13. D. Kumar, N. M. Kumar, B. Noel, and K. Shah, "A Series of 2-Arylamino-5-(indolyl)-1,3,4-thiadiazoles as Potent Cytotoxic Agents," *European Journal of Medicinal Chemistry* 55 (2012): 432–438, https://doi.org/10.1016/j.ejmech.2012.06.047.

14. K. M. Dawood, T. M. A. Eldebss, H. S. A. El-Zahabi, M. H. Yousef, and P. Metz, "Synthesis of Some New Pyrazole-Based 1,3-Thiazoles and 1,3,4-Thiadiazoles as Anticancer Agents," *European Journal of Medicinal Chemistry* 70 (2013): 740–749, https://doi.org/10.1016/j.ejmech.2013.10.042.

15. A. Husain, M. Rashid, R. Mishra, S. Parveen, D.-S. Shin, and D. Kumar, "Benzimidazole Bearing Oxadiazole and Triazolo-Thiadiazoles Nucleus: Design and Synthesis as Anticancer Agents," *Bioorganic & Medicinal Chemistry Letters* 22 (2012): 5438–5444, https://doi.org/10.1016/j.bmcl.2012.07.038.

16. W. Rzeski, J. Matysiak, and M. Kandefer-Szerszeń, "Anticancer, Neuroprotective Activities and Computational Studies of 2-Amino-1,3,4-thiadiazole Based Compound," *Bioorganic & Medicinal Chemistry* 15 (2007): 3201–3207, https://doi.org/10.1016/j.bmc.2007.02.041.

17. V. Kakekochi, U. Kumar D, N. P.p, and K. Chandrasekharan, "An Investigation on Photophysical and Third-Order Nonlinear Optical Properties of Novel Thermally-Stable Thiophene–Imidazo [2,1-b][1,3,4] Thiadiazole Based Azomethines," *Dyes and Pigments* 167 (2019): 216–224, https://doi.org/10.1016/j.dyepig.2019.04.033.

18. M. Dagli, M. Er, T. Karakurt, A. Onaran, H. Alici, and H. Tahtaci, "Synthesis, Characterization, Antimicrobial Evaluation, and Computational Investigation of Substituted Imidazo[2,1-b][1,3,4]thiadiazole Derivatives," *ChemistrySelect* 5 (2020): 11753–11763, https://doi.org/10.1002/slct.202002821.

19. S. S. Karki, K. Panjamurthy, S. Kumar, et al., "Synthesis and Biological Evaluation of Novel 2-Aralkyl-5-substituted-6-(4′-fluorophenyl)-imidazo[2,1-b][1,3,4]thiadiazole Derivatives as Potent Anticancer Agents," *European Journal of Medicinal Chemistry* 46 (2011): 2109–2116, https://doi.org/10.1016/j.ejmech.2011.02.064.

20. M. Bakherad, A. Keivanloo, M. Tajbakhsh, and T. A. Kamali, "Synthesis of 6-Benzylimidazo[2,1-b][1,3]thiazole During Sonogashira Coupling," *Synthetic Communications* 40 (2009): 173–178, https://doi.org/10.1080/00397910802573155.

21. S. Kumar, V. Gopalakrishnan, M. Hegde, et al., "Synthesis and Antiproliferative Activity of Imidazo[2,1-b][1,3,4]thiadiazole Derivatives," *Bioorganic & Medicinal Chemistry Letters* 24 (2014): 4682–4688, https://doi.org/10.1016/j.bmcl.2014.08.032.

22. S. Kumar, M. Hegde, V. Gopalakrishnan, et al., "2-(4-Chlorobenzyl)-6-arylimidazo[2,1-b][1,3,4]thiadiazoles: Synthesis, Cytotoxic Activity and Mechanism of Action," *European Journal of Medicinal Chemistry* 84 (2014): 687–697, https://doi.org/10.1016/j.ejmech.2014.07.054.

23. A. K. Gadad, S. S. Karki, V. G. Rajurkar, and B. A. Bhongade, "Synthesis and Biological Evaluation of 5-Formyl-6-arylimidazo(2,1-b)-1,3,4-thiadiazole-2-N-(dimethylaminomethino)sulfonamides as Antitumor Agents," *Arzneimittelforschung* 49 (1999): 858–863, https://doi.org/10.1055/s-0031-1300515.

24. M. Hegde, S. S. Karki, E. Thomas, et al., "Novel Levamisole Derivative Induces Extrinsic Pathway of Apoptosis in Cancer Cells and

Inhibits Tumor Progression in Mice," *PLoS One* 7, no. 9 (2012): 1–13, https://doi.org/10.1371/journal.pone.0043632.

25. B. Choodamani, K. G. Cano Hernandez, S. Kumar, et al., "Synthesis, Molecular Docking and Preliminary Antileukemic Activity of 4-Methoxybenzyl Derivatives Bearing Imidazo[2,1-b][1, 3, 4]thiadiazole," *Chemistry & Biodiversity* 18 (2021): e2000800, https://doi.org/10.1002/cbdv.202000800.

26. R. Roskoski, Jr., "A Historical Overview of Protein Kinases and Their Targeted Small Molecule Inhibitors," *Pharmacological Research* 100 (2015): 1–23, https://doi.org/10.1016/j.phrs.2015.07.010.

27. L. Le Corre, A.-L. Girard, J. Aubertin, et al., "Synthesis and Biological Evaluation of a Triazole-Based Library of Pyrido[2,3-d]pyrimidines as FGFR3 Tyrosine Kinase Inhibitors," *Organic & Biomolecular Chemistry* 8 (2010): 2164–2173, https://doi.org/10.1039/B923882D.

28. M. Er, H. Tahtaci, T. Karakurt, and A. Onaran, "Novel Substituted Imidazo[2,1-b][1,3,4]thiadiazole Derivatives: Synthesis, Characterization, Molecular Docking Study, and Investigation of Their In Vitro Antifungal Activities," *Journal of Heterocyclic Chemistry* 56 (2019): 2555–2570, https://doi.org/10.1002/jhet.3653.

29. G. Gorgisen, D. Ozes, S. Pehlivanoglu, et al., "Differential Expression and Activation of Epidermal Growth Factor Receptor 1 (EGFR1), ERK, AKT, STAT3, and TWIST1 in Nonsmall Cell Lung Cancer (NSCLC)," *Experimental Lung Research* 39 (2013): 387–398, https://doi.org/10.3109/01902148.2013.831960.

30. Z.-Q. Zhao, Z.-Y. Yu, J. Li, and X.-N. Ouyang, "Gefitinib Induces Lung Cancer Cell Autophagy and Apoptosis via Blockade of the PI3K/AKT/mTOR Pathway," *Oncology Letters* 12 (2016): 63–68, https://doi.org/10.3892/ol.2016.4606.

31. A. A. Hamid, H. J. Essa, and A. H. Dawood, "Synthesis, Characterization and Biological Activity Study of Metronidazole-Thiadiazole derivatives," *International Journal of Pharmtech Research* 9, no. 8 (2016): 428–438.

32. M. D. Hanwell, D. E. Curtis, D. C. Lonie, T. Vandermeersch, E. Zurek, and G. R. Hutchison, "Avogadro: An Advanced Semantic Chemical Editor, Visualization, and Analysis Platform," *Journal of Cheminformatics* 4 (2012): 1–17, https://doi.org/10.1186/1758-2946-4-17.

33. S. Yoshikawa, M. Kukimoto-Niino, L. Parker, et al., "Structural Basis for the Altered Drug Sensitivities of Non-Small Cell Lung Cancer-Associated Mutants of Human Epidermal Growth Factor Receptor," *Oncogene* 32 (2013): 27–38, https://doi.org/10.1038/onc.2012.21.

34. D. Brattström, K. Wester, M. Bergqvist, et al., "HER-2, EGFR, COX-2 Expression Status Correlated to Microvessel Density and Survival in Resected Non-Small Cell Lung Cancer," *Acta Oncologica* 43, no. 1 (2004): 80–86, https://doi.org/10.1080/02841860310017441.

35. M. T. Sandri, H. A. Johansson, L. Zorzino, et al., "Serum EGFR and Serum HER-2/neu Are Useful Predictive and Prognostic Markers in Metastatic Breast Cancer Patients Treated With Metronomic Chemotherapy," *Cancer* 110 (2007): 509–517, https://doi.org/10.1002/cncr.22825.

36. S.-P. Leung, O. L. Griffith, H. Masoudi, et al., "Clinical Utility of Type 1 Growth Factor Receptor Expression in Colon Cancer," *American Journal of Surgery* 195 (2008): 604–610, https://doi.org/10.1016/j.amjsurg.2007.12.032.

37. J. R. Grandis, M. F. Melhem, W. E. Gooding, et al., "Levels of TGF-α and EGFR Protein in Head and Neck Squamous Cell Carcinoma and Patient Survival," *JNCI: Journal of the National Cancer Institute* 90 (1998): 824–832, https://doi.org/10.1093/jnci/90.11.824.

38. K. K. Ang, B. A. Berkey, X. Tu, et al., "Impact of Epidermal Growth Factor Receptor Expression on Survival and Pattern of Relapse in Patients With Advanced Head and Neck Carcinoma," *Cancer Research* 62 (2002): 7350–7356.

39. E. Coudert, S. Gehant, E. De Castro, et al., "Annotation of Biologically Relevant Ligands in UniProtKB Using ChEBI," *Bioinformatics* 39 (2023): btac793, https://doi.org/10.1093/bioinformatics/btac793.

40. S. Jo, T. Kim, V. G. Iyer, and W. Im, "CHARMM-GUI: A Web-Based Graphical User Interface for CHARMM,," *Journal of Computational Chemistry* 29 (2008): 1859–1865, https://doi.org/10.1002/jcc.20945.

41. G. M. Morris, R. Huey, W. Lindstrom, et al., "AutoDock4 and AutoDockTools4: Automated Docking With Selective Receptor Flexibility," *Journal of Computational Chemistry* 30 (2009): 2785–2791, https://doi.org/10.1002/jcc.21256.

42. D. S. Biovia, *Discovery Studio Modeling Environment* (SanDiego: Dassault Systèmes, 2024).

43. I. Ozcan, S. Akkoc, H. Alici, S. Capanlar, O. Sahin, and H. Tahtaci, "Novel Thioether-Bridged 2,6-Disubstituted and 2,5,6-Trisubstituted Imidazothiadiazole Analogues: Synthesis, Antiproliferative Activity, ADME, and Molecular Docking Studies," *Chemistry & Biodiversity* 20 (2023): e202200884, https://doi.org/10.1002/cbdv.202200884.

44. W. S. Alwan, R. Karpoormath, M. B. Palkar, et al., "Novel Imidazo[2,1-b]-1,3,4-thiadiazoles as Promising Antifungal Agents Against Clinical Isolate of *Cryptococcus neoformans*," *European Journal of Medicinal Chemistry* 95 (2015): 514–525, https://doi.org/10.1016/j.ejmech.2015.03.021.

45. K. Kiymaz and S. Uysal, "The Synthesis and Characterization of Pyridine Cored Dentrimeric s-Triazine Schiff Bases: Investigation of Their [Msalen/Salophen](M = Cr^{3+}, Fe^{3+}, Co^{3+} and Zr^{4+}) Capped Complexes," *Journal of Molecular Structure* 1271 (2023): 134029, https://doi.org/10.1016/j.molstruc.2022.134029.

46. H. Tunel, M. Er, H. Alici, A. Onaran, T. Karakurt, and H. Tahtaci, "Synthesis, Structural Characterization, Biological Activity, and Theoretical Studies of Some Novel Thioether-Bridged 2,6-Disubstituted Imidazothiadiazole Analogues," *Journal of Heterocyclic Chemistry* 58 (2021): 1321–1343, https://doi.org/10.1002/jhet.4260.

47. O. Khalid, M. Salah, A. H. Mirghani, H. Tahtaci, A. Coskun, and S. Uysal, "Synthesis of Bilaterally Thiadiazole Substituted vic-Dioxime Ligands and Investigation of Their Polymeric Metal Complexes," *Journal of Molecular Structure* 1318 (2024): 139234, https://doi.org/10.1016/j.molstruc.2024.139234.

48. A. S. Otaiwi, A. H. Mirghani, H. E. Bostancı, A. Coskun, H. Tahtaci, and S. Uysal, "Synthesis and Characterization of Oxime Derivatives and Their Some Transition Metal Complexes With Thiadiazole Groups: Biological Activities, and Molecular Docking Studies of the Ligands," *ChemistrySelect* 9 (2024): e202400863, https://doi.org/10.1002/slct.202400863.

49. Ş. Uysal and Z. Erdem Koç, "The Synthesis and Characterization of (MSalen/salophen/saldeta/salpy) [M = Fe(III) or Cr(III)] Capped Heteromultinuclear Schiff Bases-Dioxime Ni(II) Complexes: Their Thermal and Magnetic Behaviours," *Journal of Molecular Structure* 1165 (2018): 14–22, https://doi.org/10.1016/j.molstruc.2018.03.101.

50. M. Wang and A. Y.-C. Chang, "Molecular Mechanism of Action and Potential Biomarkers of Growth Inhibition of Synergistic Combination of Afatinib and Dasatinib Against Gefitinib-Resistant Non-Small Cell Lung Cancer Cells," *Oncotarget* 9, no. 23 (2018): 16533–16546, https://doi.org/10.18632/oncotarget.24814.

51. Z. Liu and W. Gao, "Overcoming Acquired Resistance of Gefitinib in Lung Cancer Cells Without T790M by AZD9291 or Twist1 Knockdown In Vitro and In Vivo," *Archives of Toxicology* 93 (2019): 1555–1571, https://doi.org/10.1007/s00204-019-02453-2.

52. W. Yao, L. Wang, H. Huang, et al., "All-Trans Retinoic Acid Reduces Cancer Stem Cell-Like Cell-Mediated Resistance to Gefitinib in NSCLC Adenocarcinoma Cells," *BMC Cancer* 20 (2020): 1–9, https://doi.org/10.1186/s12885-020-06818-0.

Supporting Information

Additional supporting information can be found online in the Supporting Information section.